Soft-Decision-Driven Sparse Channel Estimation and Turbo Equalization for MIMO Underwater Acoustic Communications

Youwen Zhang, Yuriy Zakharov, *Senior Member, IEEE*, Jianghui Li, *Member, IEEE*

***Abstract*—Multi-input multi-output (MIMO) detection based on turbo principle has been shown to provide a great enhancement in the throughput and reliability of underwater acoustic (UWA) communication systems. Benefits of the iterative detection in MIMO systems, however, can be obtained only when a high quality channel estimation is ensured. In this paper, we develop a new soft-decision-driven sparse channel estimation and turbo equalization scheme in the triply selective MIMO UWA. First, the Homotopy recursive least square dichotomous coordinate descent (Homotopy RLS-DCD) adaptive algorithm, recently proposed for sparse single-input single-output (SISO) system identification, is extended to adaptively estimate rapid time-varying MIMO sparse channels. Next, the more reliable *a posteriori* soft-decision symbols, instead of the hard decision symbols or the *a priori* soft-decision symbols, at the equalizer output, are not only feedback to the Homotopy RLS-DCD based channel estimator but also to the minimum mean-square-error (MMSE) equalizer. As the turbo iterations progress, the accuracy of channel estimation and the quality of the MMSE equalizer are improved gradually, leading to the enhancement in the turbo equalization performance. This also allows the reduction in pilot overhead. The proposed receiver has been tested by using the data collected from the SHLake2013 experiment. The performance of the receiver is evaluated for various modulation schemes, channel estimators and MIMO sizes. Experimental results demonstrate that the proposed *a posteriori* soft-decision-driven sparse channel estimation based on the Homotopy RLS-DCD algorithm and turbo equalization offer considerable improvement in system performance over other turbo equalization schemes.**

***Index Terms*—*A posteriori* soft-decision, *a priori* soft-decision, channel estimation, DCD iterations, Homotopy iterations, multiple-input multiple-output (MIMO), recursive least-squares (RLS), sparse channel, turbo equalization, underwater acoustic communication.**

I. Introduction

In recent years, the terrestrial wireless communication has made great achievements, However, wireless communication underwater, more specifically, the underwater acoustic communication, is still facing significant challenges incurred by the harsh underwater acoustic propagation environment [1]–[8]. Unlike the terrestrial radio channel, the UWA channel is featured by frequency-dependent limited bandwidth, long delay spread and rapid time variation due to severe Doppler effects (caused by the low speed of sound in water), leading to relatively low data rates in a range between a few bits/s (bps) to several tens of kbits/s ($kbps$) and often unsatisfied performance. The UWA channel has been regarded as one of the most difficult channels for communications [8], [10].

Generally, two families of modulation techniques, single-carrier modulation and multicarrier modulation, are widely investigated in UWA communications [10], [12]–[14]. These two types of modulation have their own advantages and disadvantages in combating the distortions incurred by the UWA channel. Single-carrier modulation schemes with time-domain equalization techniques enjoy high spectral efficiency and robust performance at the cost of a high receiver complexity due to the fast time-varying long multipath spread and Doppler spread [1], [9]–[11], [19]–[21]. Multicarrier modulation schemes, such as the orthogonal frequency-division multiplexing (OFDM), have a substantial advantage in combating long multipath spread with a relatively low-complexity equalization by utilizing the cyclic prefix (CP). Unfortunately, the block-wise processing used in OFDM systems usually requires the assumption of time-invariant or quasi-static channel. In rapidly varying UWA channels, the severe intercarrier interference (ICI) due to the Doppler spread significantly degrades the performance of OFDM systems [12], [13], [15], [17], [18]. On the other hand, the high peak-to-average power ratio (PAPR) is another problem in OFDM systems, especially for battery-powered underwater platforms [16].

To boost the throughput and robustness of communications over time-varying triply (space-time-frequency) selective underwater acoustic channels, the MIMO transmission coupled with turbo equalization (TEQ), i.e. iterative equalization and decoding, has been recently recognized as a powerful and promising solution for UWA communications [19]–[23], [25]–[27], [31]–[38]. Usually, the TEQ can be performed in either time or frequency domain according to the requirements to the receiver structure and computational complexity. In this work, we focus on the single-carrier UWA communication with time-domain TEQ [19]–[22], [25]–[27], [35]–[37]; for details on the frequency-domain TEQ for single-carrier or OFDM systems, we refer the reader to [27], [31]–[34]. There have emerged many time-domain TEQ schemes in the field of UWA communications. The TEQ schemes with the linear structure have a suboptimal performance, but relatively low complexity. They generally fall into two classes: 1) the direct-adaptive based TEQ (DA-TEQ), with direct application of adaptive filters to

Youwen Zhang is with the Acoustic Science and Technology Laboratory and the College of Underwater Acoustic Engineering, Harbin Engineering University, Harbin, Heilongjiang, 150001, China. Email: zhangyouwen@hrbeu.edu.cn.

Yuriy Zakharov is with the Department of Electronic Engineering, University of York, York, YO10 5DD, UK. Email: yury.zakharov@york.ac.uk.

Jianghui Li is with the Institute of Sound and Vibration Research, University of Southampton, U.K., e-mail: J.Li@soton.ac.uk.

the received signal to estimate the transmitted symbols [20]–[23], [25], [35]–[37], and 2) the channel-estimate based TEQ (CE-TEQ), with explicit channel estimation performed firstly, and then the TEQ coefficients determined from the channel estimate [20], [38].

As shown in many research works in the field of UWA TEQs, the channel estimation errors in CE-TEQs and the adaptive filter adjustment errors in DA-TEQs have a significant impact on the performance of receivers [20], [36]–[38]. In [20], the behavior of both CE-TEQ and DA-TEQ based on the Least Mean Square (LMS) adaptive algorithm in the presence of channel estimation errors and adaptive filter adjustment errors were compared by theoretical analysis, simulation and processing the experimental data. The data reuse and fixed taps sparsification techniques were used to improve the convergence of the LMS algorithm. For both single-input multi-output (SIMO) and MIMO configurations, extensive at-sea experiments have shown that, in some setups, the DA-TEQ scheme outperforms the CE-TEQ scheme, which is a counterintuitive and contradicts to the theoretical analysis and simulation. In [21], an LMS-based DA-TEQ scheme for high order modulations (up to 32QAM) coupled with the symbol-based timing recovery and Doppler compensation was proposed for highly-mobile SIMO UWA communications. At-sea experiments show that data rates up to 20 $kbps$ can be achieved with a satisfied performance for relative velocities up to 2 m/s. Further results with higher data rates up to 24 $kbps$ over ranges greater than 1 km are presented in [22]. In [23], an DA-TEQ scheme with sparsity-aware Improved Proportional Normalized LMS (IPNLMS) adaptive filter [7], [24] for the SIMO setup shows an improved performance compared to the LMS based DA-TEQ. In [25], the authors developed a soft adaptive turbo equalizer that incorporates the soft information from the decoder into the adaptation loop. In the context of DA-TEQ, the recursive expected least squares (RELS) adaptive algorithm, which could take advantage of the soft information as opposed to the hard information, is used in the turbo equalizer. Unlike the works conducted in [20]–[23], *a priori* soft-decisions (SDs) from the decoder are also feedback to update the adaptive filter coefficients, leading to a performance robust to the error propagation (EP) incurred by the hard decision feedback. In [38], an CE-TEQ scheme with iterative channel estimation and turbo equalization for MIMO UWA communication was proposed. By utilizing the IPNLMS algorithm that takes the channel sparsity into account instead of the LMS or block-wise least squares (LS) algorithms in the iterative channel estimation, the conclusion that the CE-TEQ scheme definitely outperforms the DA-TEQ is verified by experimental results. These at-sea experimental results are consistent with the theoretical analysis and simulation results presented in [20]. In [37], an efficient DA-TEQ scheme for MIMO UWA communications was proposed. Different from existing DA-TEQ schemes, the *a posteriori* soft-decision of the TEQ output is feedback to the adaptive filter and SIC. To cope with the slow convergence that is inherent in NLMS and IPNLMS algorithms, the same data reuse technique as in [20] was embedded in the turbo iteration loop. Experimental results demonstrate superiority of the *a posteriori* SDs in TEQ schemes against utilizing the hard decision or the *a priori* SDs. Built on the above insight, the LMS-type or enhanced LMS-type adaptive algorithms were widely used in these DA-TEQ and CE-TEQ schemes due to their low complexity. The slower convergence speed of LMS-based algorithms, however, limits their application in the rapid time-varying MIMO UWA channels. It is well known that recursive least squares (RLS) adaptive algorithms provide significantly faster convergence at the expense of a higher complexity when compared to LMS adaptive algorithms [20].

In this paper, motivated by the works in [27], [37], [38], we propose a soft-decision-driven iterative channel estimation and turbo equalization CE-TEQ scheme for single carrier MIMO UWA communications. As compared to existing works, our main contributions are summarized below:

1) A low complexity RLS-type algorithm for SISO sparse system identification with Homotopy, dichotomous coordinate descent (DCD) and reweighting iterations, exponential-weighted Homotopy RLS-DCD (EW-HRLS-DCD) algorithm [28], [29], is extended to estimate time-varying sparse MIMO UWA channels. The proposed adaptive channel estimator based on the EW-HRLS-DCD algorithm, can capture the inherent sparsity of the MIMO UWA channel, leading to significant improvement in the performance compared with the classical RLS algorithm and other sparse RLS algorithms [30]. Its complexity is only linear in the length of the estimated channel. The proposed estimator is based on DCD iterations well suited to implementation on real-time platforms with finite precision such as the DSP and FPGA platforms.
2) More reliable *a posteriori* soft decisions, instead of the hard decisions or the *a priori* soft decisions, from the equalizer output are incorporated into the proposed EW-HRLS-DCD-based channel estimator and MMSE equalizer. The proposed TEQ significantly outperforms existing TEQs based on the LMS-type algorithms including those with data reuse and soft-decisions. Note that the data reuse techniques will incur a high processing latency if the total number of repetition for data reuse is large.
3) The performance of the proposed receiver was tested in the SHLake2013 lake trial, at a communication distance of 2 km. We show that the proposed scheme can achieve a substantial performance gain over the IPNLMS- and RLS-based TEQ schemes for all MIMO setups. For an 2×4 MIMO configuration with QPSK modulation, the proposed scheme can successfully retrieve 136 data packets out of 144 with a 20% training overhead. For an 2×8 MIMO configuration with 8PSK modulation, the best detection performance can be achieved by the proposed scheme, while the IPNLMS-based scheme experiences the convergence problem and can not obtain a satisfying performance.

The remainder of the paper is organized as follows. In Section II, the time-varying frequency-selective MIMO system model is presented. In Section III, the channel estimation

based on the conventional RLS algorithm for MIMO systems is reviewed. A new low-complexity sparse MIMO channel estimator, based on the exponential-weighted Homotopy RLS-DCD adaptive filtering, is proposed by solving a sequence of auxiliary normal equations instead of solving the standard normal system utilized in the conventional RLS algorithm. Section IV presents an iterative MIMO receiver with channel estimation and equalization driven by the *a posteriori* soft decisions. The complexity of proposed channel estimator is presented in Section V. Section VI demonstrates the performance of the proposed scheme by experimental results. Conclusions are drawn in Section VII.

Notation: Matrices and vectors are represented by bold letters in capital cases and small cases, respectively. $\mathbf{X} \in \mathbb{C}^{N\times M}$ denotes a complex-valued $(N \times M)$ matrix, where $\mathbb{C}$ represents the complex field; the operators $\mathbf{X}^*$, $\mathbf{X}^{\mathrm{T}}$, $\mathbf{X}^{\dagger}$, $\mathbf{X}^{-1}$, $|\mathbf{X}|$, $\|\mathbf{X}\|_F$ denote the complex conjugate, transpose, Hermitian transpose, inverse, determinant, and Frobenius norm of $\mathbf{X}$, respectively. The vectorisation operator $\mathrm{vec}[\mathbf{X}]$ creates a column vector by stacking all columns of $\mathbf{X}$ in a left-to-right fashion. $\mathbb{R}$ and $\mathbb{R}_+$ denote the set of real numbers and Nonnegative sets of real numbers, respectively. The empty set is represented by $\varnothing$. An m-dimensional identity matrix is denoted by $\mathbf{I}_m$. The ℓ_p vector norm is defined as $\|\mathbf{x}\|_p = \left(\sum_i |x_i|^p\right)^{1/p}$, where x_i are elements (entries) of $\mathbf{x}$. $\mathcal{CN}(\boldsymbol{\mu}, \boldsymbol{\Sigma})$ represents a multivariate complex-valued Gaussian distribution with mean $\boldsymbol{\mu}$ and covariance $\boldsymbol{\Sigma}$. I and I^c denote the support of non-zero elements and its complement. $\Re\{\cdot\}$ denotes the real part of a complex number. $\mathbb{E}\{\cdot\}$ denotes the mathematical expectation.

II. MIMO System Model

We consider an $N \times M$ MIMO with bit-interleaved coded modulation (BICM) single-carrier UWA communication system in which N transducers are used at the transmitter and M hydrophones are used at the receiver. The structure of the transmitter considered here is shown in Fig. 1. The binary information sequence stream $\{\mathbf{a}_n\}_{n=1}^N$ represents the input bits to the N parallel transmit branches. On the n-th transmit branch, the information bits $\mathbf{a}_n$ are encoded by a rate R_c channel encoder, producing the encoded bit sequence $\mathbf{b}_n$. The n-th random interleaver Π_n is used to permute the encoded bits $\mathbf{b}_n$, producing the interleaved and encoded bits $\mathbf{c}_n$. For a digital modulation scheme with a constellation size of 2^J, every J interleaved bits from $\mathbf{c}_n$, $\mathbf{c}_{n,k} \triangleq [c_n^1(k) \quad c_n^2(k) \cdots c_n^J(k)]$, $c_n^j(k) \in \{0, 1\}$, are mapped to 2^J-ary constellation set $\mathcal{A} = \{\alpha_1, \alpha_2, \cdots, \alpha_{2^J}\}$, producing one modulation symbol $x_n(k)$. In the following, we denote $x_n(k)$ as a symbol transmitted by the n-th transducer at time k.

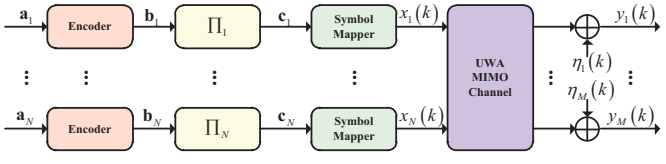

Fig. 1. The block diagram of the transmitter architecture. $\{\Pi_n\}_{n=1}^N$ denote N interleavers.

The frequency-selective channel is modeled by a sample-space tapped delay line. We assume that the maximum multipath delay in symbol intervals is at most P. At time k, the equivalent discrete-time baseband signal received on the m-th hydrophone is given as

$$y_m(k) = \sum_{p=0}^{P-1} \sum_{n=1}^{N} h_{m,n}^p(k) x_n(k-p) + \eta_m(k), \tag{1}$$

where $h_{m,n}^p(k) \in \mathbb{C}$ represents the p-th tap of the length-P equivalent channel impulse response between the n-th transducer and the m-th hydrophone at time instant k, and $\eta_m(k)$ is the additive noise modeled by zero-mean complex Gaussian circulary symmetrical random variable and received at the m-th hydrophone at time k. The signal vector received by M hydrophones, $\mathbf{y}(k) \triangleq [y_1(k), y_2(k), \ldots, y_M(k)]^T$, can be represented as

$$\mathbf{y}(k) = \sum_{p=0}^{P-1} \mathbf{H}_p(k)\mathbf{x}(k-p) + \boldsymbol{\eta}(k), \tag{2}$$

where

$$\mathbf{x}(k) \triangleq [x_1(k), x_2(k), \ldots, x_N(k)]^T \in \mathbb{C}^{N\times 1} \tag{3}$$

$$\boldsymbol{\eta}(k) \triangleq [\eta_1(k), \eta_2(k), \ldots, \eta_M(k)]^T \in \mathbb{C}^{M\times 1} \tag{4}$$

$$\mathbf{H}_p(k) \triangleq \begin{bmatrix} h_{1,1}^p(k) & h_{1,2}^p(k) & \cdots & h_{1,N}^p(k) \\ h_{2,1}^p(k) & h_{2,2}^p(k) & \cdots & h_{2,N}^p(k) \\ \vdots & \vdots & \ddots & \vdots \\ h_{M,1}^p(k) & h_{M,2}^p(k) & \cdots & h_{M,N}^p(k) \end{bmatrix} \in \mathbb{C}^{M\times N}, \tag{5}$$

$\boldsymbol{\eta}(k)$ is the noise vector with covariance $\mathbb{E}\{\boldsymbol{\eta}(k)\boldsymbol{\eta}^{\dagger}(k)\} = \sigma_\eta^2 I_M$. One can further rewrite the received signals as

$$\mathbf{y}(k) = \mathbf{H}(k)\boldsymbol{\chi}(k) + \boldsymbol{\eta}(k) \tag{6}$$

where

$$\mathbf{H}(k) \triangleq [\mathbf{H}_0(k), \mathbf{H}_1(k), \ldots, \mathbf{H}_{P-1}(k)] \in \mathbb{C}^{M\times L} \tag{7}$$

$$\boldsymbol{\chi}(k) \triangleq [\mathbf{x}^T(k), \mathbf{x}^T(k-1), \ldots, \mathbf{x}^T(k-P+1)]^T \tag{8}$$

$$\in \mathbb{C}^{L\times 1} \tag{9}$$

with $L = NP$. At time k, the transmitted signal vector, $\boldsymbol{\chi}(k)$, is formed by stacking the past $P-1$ symbols together with the current signal vector $\mathbf{x}(k)$.

III. MIMO Channel Estimation

A. Structure of Adaptive MIMO Channel Estimation

The $(N\times M)$ MIMO channel is modeled as (NM) finite impulse response (FIR) filters [35], [38]. Fig. 2 depicts the general structure of MIMO channel estimation based on adaptive algorithms. At the n-th transmit branch, the n-th training signal vector is defined as $\mathbf{x}_n(k) \triangleq [x_{n,k}, x_{n,k-1}, \ldots, x_{n,k-P+1}]^T$, where k is the time index during the adaptive channel estimation. $\mathbf{x}(k) \triangleq [\mathbf{x}_1^T(k), \mathbf{x}_2^T(k), \ldots, \mathbf{x}_N^T(k)]^T$ is the concatenated training signal vector of all the N branches.

An adaptive $N\times M$ MIMO channel estimation problem can be transformed into M equivalent adaptive $N \times 1$ multi-input

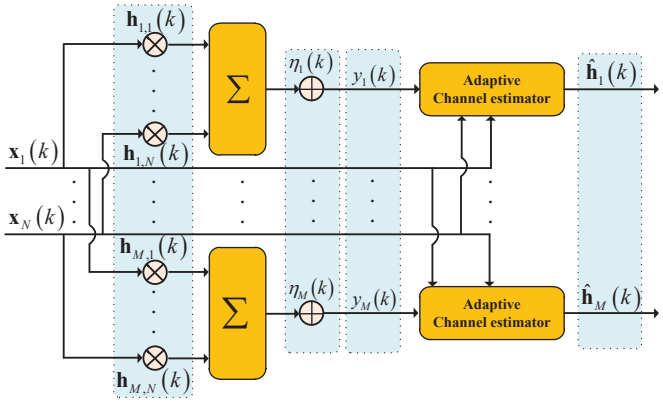

Fig. 2. Structure of adaptive $N \times M$ MIMO channel estimation.

single-output (MISO) channel estimation problems. At the m-th hydrophone, *a priori* error of adaptive channel estimator, $e_m(k)$, is represented as $e_m(k) = y_m(k) - \mathbf{x}^\dagger(k)\hat{\mathbf{h}}_m(k)$ given the received signal $y_m(k)$ and training signal vector $\mathbf{x}(k)$. Depending on various design criteria such as the complexity and tracking performance, many adaptive algorithms can be adopted to find the estimate $\hat{\mathbf{h}}_m(k)$. The adaptive MIMO channel estimators presented in following subsections are all based on the structure shown in Fig. 2.

B. Conventional RLS Algorithm

At time instance k, the task of the channel estimator is to estimate the time-varying channel matrix $\mathbf{H}(k)$ by using known training symbols and the received signal [39], [41], [42]. The RLS algorithm is one of the well-known adaptive algorithms. Generally, the RLS-type algorithms fall into two classes according to the adopted window function: the exponential-weighted RLS (EW-RLS) algorithms and sliding-window RLS (SW-RLS) algorithms [39]. Here, we consider the EW-RLS algorithms since they have lower complexity. In the EW-RLS algorithm, an exponentially-weighted mean-squared error (MSE) $\varepsilon(k)$ is minimized as follows [39], [41], [42]

$$\min_{\hat{\mathbf{H}}(k)} \left\{ \varepsilon(k) \triangleq \sum_{l=1}^{k} \lambda^{k-l} \left\| \mathbf{y}(l) - \hat{\mathbf{H}}(k)\boldsymbol{\chi}(l) \right\|_2^2 \right\} \tag{10}$$

or is given by (11), shown at the bottom of the next page. We define

$$\mathbf{Y}(k) \triangleq [\mathbf{y}(1), \mathbf{y}(2), \ldots, \mathbf{y}(k)] \in \mathbb{C}^{M\times k} \tag{12}$$

$$\boldsymbol{\Lambda}(k) \triangleq diag\left[\lambda^{k-1}, \lambda^{k-2}, \ldots, \lambda^0\right] \in \mathbb{R}^{k\times k} \tag{13}$$

$$\mathbf{X}(k) \triangleq [\boldsymbol{\chi}(1), \boldsymbol{\chi}(2), \ldots, \boldsymbol{\chi}(k)] \in \mathbb{C}^{L\times k} \tag{14}$$

The matrix $\boldsymbol{\Lambda}(k)$ provides the exponential windowing. To accommodate the time-varying channel, the RLS forgetting factor λ, which controls the trade-off between the good tracking ability and the noise sensitivity, must be taken in $(0\ 1]$. In practice, the forgetting factor should be adjusted under different channel conditions such as the channel coherence time and Signal-to-Noise ratio (SNR) [1], [39].

With the direct block-wise LS solution, at time k, the channel estimate is given by [42], [43]

$$\hat{\mathbf{H}}(k) = \mathbf{Y}(k)\boldsymbol{\Lambda}(k)\mathbf{X}^\dagger(k)\left(\mathbf{X}(k)\boldsymbol{\Lambda}(k)\mathbf{X}^\dagger(k)\right)^{-1} \tag{15}$$

Since the direct matrix inverse operation is adopted in the direct LS solution, the complexity of the block-wise LS channel estimation algorithm is $\mathcal{O}(L^3)$, i.e., it is prohibitively high, especially for UWA channels with long delay spreads.

However, the EW-RLS algorithm can calculate the solution using recursions as follows [39], [41], [42]:

$$\boldsymbol{\zeta}(k) = \frac{1}{\lambda}\boldsymbol{\Phi}(k-1)\boldsymbol{\chi}(k) \in \mathbb{C}^{L\times 1} \tag{16}$$

$$\boldsymbol{e}(k) = \mathbf{y}(k) - \hat{\mathbf{H}}(k-1)\boldsymbol{\chi}(k) \in \mathbb{C}^{M\times 1} \tag{17}$$

$$\boldsymbol{\Phi}(k) = \frac{1}{\lambda}\boldsymbol{\Phi}(k-1) - \frac{\boldsymbol{\zeta}(k)\boldsymbol{\zeta}^\dagger(k)}{1+\boldsymbol{\zeta}^\dagger(k)\boldsymbol{\chi}(k)} \in \mathbb{C}^{L\times L} \tag{18}$$

$$\hat{\mathbf{H}}(k) = \hat{\mathbf{H}}(k-1) + \frac{\boldsymbol{e}(k)\boldsymbol{\zeta}^\dagger(k)}{1+\boldsymbol{\zeta}^\dagger(k)\boldsymbol{\chi}(k)} \in \mathbb{C}^{M\times L} \tag{19}$$

with $\hat{\mathbf{H}}(0) = \mathbf{0}_{M\times L}$ and $\boldsymbol{\Phi}(0) = \delta\mathbf{I}_L$, where $\delta > 0$ is a regularization parameter.

Since $\boldsymbol{\Phi}(k)$ in (18) is computed recursively thus avoiding the direct matrix inversion, the EW-RLS complexity is reduced from $\mathcal{O}(L^3)$ to $\mathcal{O}(L^2)$ arithmetic operations per sample [39].

C. Recursive Solution of RLS Normal Equations for MIMO Channel Model

Most conventional RLS or fast RLS algorithms are based on the matrix inverse, which results in the problem of numerical instability when implemented with finite precision [39]. In [44], to overcome the high complexity and numerical instability problems, a new formulation of the RLS problem in terms of a sequence of auxiliary normal equations with respect to increments of the filter weights was developed to find a solution to the normal equation given by

$$\mathbf{H}(k)\mathbf{R}(k) = \mathbf{B}(k) \tag{20}$$

where $\mathbf{R}(k) = \boldsymbol{\chi}(k)\boldsymbol{\Lambda}(k)\boldsymbol{\chi}^\dagger(k)$ and $\mathbf{B}(k) = \mathbf{y}(k)\boldsymbol{\Lambda}(k)\boldsymbol{\chi}^\dagger(k)$ are the $L \times L$ autocorrelation matrix of the input signal and $M \times L$ matrix of cross-correlation between the input signal and desired signal, respectively. The matrices $\mathbf{R}(k)$ and $\mathbf{B}(k)$ are known, whereas the matrix $\mathbf{H}(k)$ should be estimated.

Let at time $k-1$ a system of equations $\mathbf{H}(k-1)\mathbf{R}(k-1) = \mathbf{B}(k-1)$ be approximately solved, and the approximate solution is $\hat{\mathbf{H}}(k-1)$. Denote

$$\mathbf{C}(k-1|k-1) = \mathbf{B}(k-1) - \hat{\mathbf{H}}(k-1)\mathbf{R}(k-1) \in \mathbb{C}^{M\times L} \tag{21}$$

and

$$\mathbf{C}(k|k-1) = \mathbf{B}(k) - \hat{\mathbf{H}}(k-1)\mathbf{R}(k) \in \mathbb{C}^{M\times L} \tag{22}$$

as residual matrices for the solution $\hat{\mathbf{H}}(k-1)$. The notation $\mathbf{C}(j|k-1)$ indicates that the residual matrix corresponds to $\mathbf{R}(j)$ and $\mathbf{B}(j)$ at time instant $j \geq k-1$, whereas the solution $\hat{\mathbf{H}}(k-1)$ corresponds to the system $\mathbf{H}(k-1)\mathbf{R}(k-1) = \mathbf{B}(k-1)$ at time instant $k-1$ [44].

For the convenience of following derivation, we denote $\Delta\mathbf{R}(k) = \mathbf{R}(k) - \mathbf{R}(k-1)$, $\Delta\mathbf{B}(k) = \mathbf{B}(k) - \mathbf{B}(k-1)$, and

$$\Delta\mathbf{H}(k) = \mathbf{H}(k) - \hat{\mathbf{H}}(k-1). \tag{23}$$

With the previously obtained solution $\hat{\mathbf{H}}(k-1)$ and the residual matrix $\mathbf{C}(k|k-1)$, our purpose is to find a solution $\hat{\mathbf{H}}(k)$ of (20). The equation (20) can be rewritten as

$$\left[\hat{\mathbf{H}}(k-1) + \Delta\mathbf{H}(k)\right]\mathbf{R}(k) = \mathbf{B}(k) \tag{24}$$

Hence, the system of equations with respect to the unknown matrix $\Delta\mathbf{H}(k)$ is represented as

$$\Delta\mathbf{H}(k)\mathbf{R}(k) = \mathbf{C}(k|k-1). \tag{25}$$

Instead of solving the original problem (20), we can find a solution $\Delta\hat{\mathbf{H}}(k)$ of the auxiliary system of equations (25), where

$$\mathbf{C}(k|k-1) = \mathbf{C}(k-1|k-1) + \Delta\mathbf{B}(k) - \hat{\mathbf{H}}(k-1)\Delta\mathbf{R}(k) \tag{26}$$

and an approximate solution of the original system (20) is obtained as

$$\hat{\mathbf{H}}(k) = \hat{\mathbf{H}}(k-1) + \Delta\hat{\mathbf{H}}(k). \tag{27}$$

For the EW-RLS problem, the $L \times L$ matrix $\mathbf{R}(k)$ and $M \times L$ matrix $\mathbf{B}(k)$ can be recursively updated as [39]

$$\mathbf{R}(k) = \lambda\mathbf{R}(k-1) + \boldsymbol{\chi}(k)\boldsymbol{\chi}^{\dagger}(k) \in \mathbb{C}^{L\times L}, \tag{28}$$

$$\mathbf{B}(k) = \lambda\mathbf{B}(k-1) + \mathbf{y}(k)\boldsymbol{\chi}^{\dagger}(k) \in \mathbb{C}^{M\times L}, \tag{29}$$

where $k > 0$, $\mathbf{R}(0) = \varrho\mathbf{I}_L$, and ϱ is a small positive number for regularization of the adaptation at the initial stage.

The residual matrix $\mathbf{C}(k|k-1)$ in equation (26) can be efficiently updated using the following relationship [44]

$$\mathbf{C}(k|k-1) = \lambda\mathbf{C}(k-1|k-1) + \mathbf{e}^{*}(k)\boldsymbol{\chi}^{T}(k), \tag{30}$$

where $\mathbf{e}(k) = \mathbf{y}(k) - \hat{\mathbf{H}}(k-1)\boldsymbol{\chi}(k)$ is the $M \times 1$ *a priori* estimation error vector.

D. Homotopy *RLS-DCD Algorithm for Time-varying MIMO Sparse Channel Estimation*

Time-varying multipath UWA communication channels often exhibit sparsity, i.e., the most entries in $\mathbf{H}(k)$ are close to zero [45]. With *a priori* information on the sparsity, some channel estimators can obtain improved performance in terms of channel tracking and computational complexity [20], [23], [37], [38], [45], [46].

Compressive sensing based sparse channel estimation techniques [47] are widely used in UWA communications [48], but the prohibitive computational complexity limits their application in MIMO UWA systems [49]. Recently, many adaptive algorithms have been developed to deal with sparse recovery problems. Unfortunately, most of these adaptive algorithms for UWA channel estimation have either a good performance but with a high complexity of at least $\mathcal{O}(L^2)$, e.g. RLS-type algorithms, or a low complexity of $\mathcal{O}(L)$ but with a low performance, e.g. LMS-type algorithms.

Here, we introduce a recently proposed algorithm, named as the exponentially-weighted Homotopy RLS-DCD algorithm [28], and extend it for estimation of time-varying MIMO sparse channels. Assume that the channel is sparse, i.e. the number S of non-zero taps in $h_{m,n}^{p}(k)$, $p = 0, \cdots, P-1$, satisfies $S \ll P$. A sparse approximation to the UWA channel response $\mathbf{H}(k)$ can be obtained by solving the following optimization problem:

$$\min_{\hat{\mathbf{H}}(k)} \left\| vec\left[\hat{\mathbf{H}}(k)\right]\right\|_0, \quad s.t.\ \varepsilon(k) \le \epsilon \tag{31}$$

where ϵ is a small positive constant, which controls the estimation error. The non-convexity of above optimization problem results in intractable computations. A convex relaxation provides a viable alternative to the non-convex problem, whereby the ℓ_0-norm, $\left\| vec\left[\hat{\mathbf{H}}(k)\right]\right\|_0$ is replaced with the ℓ_1-norm $\left\| vec\left[\hat{\mathbf{H}}(k)\right]\right\|_1$. Various adaptive filters can solve this problem in a computationally efficient way [50]–[52].

The adaptive filter finds a complex-valued tap-weight matrix $\hat{\mathbf{H}}(k)$, which, at every time instant *k*, minimizes the cost function $\varepsilon'(k)$:

$$\min_{\hat{\mathbf{H}}(k)} \left\{ \varepsilon'(k) \triangleq \frac{1}{\sigma^2}\varepsilon(k) + f_p\left[\hat{\mathbf{H}}(k)\right] \right\}, \tag{32}$$

where the first term of $\varepsilon'(k)$ is the LS error of the solution and the second term $f_p\left[\hat{\mathbf{H}}(k)\right]$ is a penalty function that incorporates *a priori* information on the solution [52]:

$$f_p\left[\hat{\mathbf{H}}(k)\right] = \tau \left\| \mathbf{w}^{T}(k) vec\left[\hat{\mathbf{H}}(k)\right]\right\|_1 \tag{33}$$

where the vector $\mathbf{w}$ contains ML positive weights $w_j(k)$ which are updated during the adaptation as [53]

$$w_j(k) = \frac{1}{|h_j(k-1)|^2 + \varsigma}, \tag{34}$$

$\varsigma > 0$ is an adjusted parameter, $h_j(k-1)$ is the j-th element in the estimated channel vector $vec(\hat{\mathbf{H}}(k-1))$. The positive scalar τ in (33) is a regularization parameter that controls the balance between the LS fitting term and the penalty term in (32).

The Homotopy algorithm minimizes the cost function $\varepsilon'(k)$ in (32). A set of homotopy iterations is performed for exponentially decreasing values of the regularization parameter vector $\boldsymbol{\tau}$: $\boldsymbol{\tau} \leftarrow \gamma\boldsymbol{\tau}$, where γ is the decreasing factor and must be taken in $(0, 1)$. If γ is close to one, a large number of homotopy iterations are needed, which result in a high complexity. In order to reduce the complexity of adaptive filtering based on the Homotopy algorithm, it is enough to perform only one homotopy iteration. For further reduction in the complexity, DCD iterations are used [44], [54].

$$\min_{\hat{\mathbf{H}}(k)} \left\{ \varepsilon(k) \triangleq \mathrm{tr}\left[\left(\mathbf{Y}(k) - \hat{\mathbf{H}}(k)\mathbf{X}(k)\right) \boldsymbol{\Lambda}(k) \left(\mathbf{Y}(k) - \hat{\mathbf{H}}(k)\mathbf{X}(k)\right)^{\dagger} \right] \right\} \tag{11}$$

TABLE I
EXPONENTIAL-WEIGHTED HOMOTOPY RLS-DCD ADAPTIVE ALGORITHM FOR MIMO CHANNEL ESTIMATION

	Input: $\boldsymbol{\chi}$, $\mathbf{y}$, $\boldsymbol{\tau}$, M, L, λ, γ, M_b, N_u, ε **Output:** $\hat{\mathbf{H}}(k)$, $\mathbf{C}(k\|k)$
Step	**Initialization:** $\hat{\mathbf{H}}(0)=\mathbf{0}$, $\{I_m=\varnothing\}_{m=1}^{M}$, $\mathbf{C}(0\|0)=\mathbf{0}$, $\mathbf{B}(0)=\mathbf{0}$, $\mathbf{R}(0)=\varepsilon\mathbf{I}_L$, $\mathbf{W}(1)=\mathbf{1}_{M\times L}$
	for $k=1$ **to** K % *loop for* K *received symbols*
1	$\mathbf{R}(k)=\lambda\mathbf{R}(k-1)+\boldsymbol{\chi}(k)\boldsymbol{\chi}^{\dagger}(k)$
2	$\mathbf{B}(k)=\lambda\mathbf{B}(k-1)+\mathbf{y}(k)\boldsymbol{\chi}^{\dagger}(k)$
3	$\mathbf{d}(k)=\hat{\mathbf{H}}(k-1)\boldsymbol{\chi}(k)$
4	$\mathbf{e}(k)=\mathbf{y}(k)-\mathbf{d}(k)$
5	$\mathbf{C}(k\|k-1)=\lambda\mathbf{C}(k-1\|k-1)+\mathbf{e}^{*}(k)\boldsymbol{\chi}^{T}(k)$
6	**for** $m=1$ **to** M % *loop for* M *hydrophones*
7	$\tau_m=\max_j\|c_{m,j}\|, 1\le j\le L$
8	$t=\arg\min_{j\in I_m}\frac{1}{2}\|h_{m,j}\|^2R_{j,j}+\Re\{h_{m,j}^{*}c_{m,j}\}-\tau_m w_{m,j}\|h_{m,j}\|$
9	**if** $\frac{1}{2}\|h_{m,t}\|^2R_{t,t}+\Re\{h_{m,t}^{*}c_{m,t}\}-\tau_m w_{m,t}\|h_{m,t}\|<0$
9.1	Remove the t-th element from I_m ($I_m\leftarrow I_m\setminus t$)
9.2	$\mathbf{c}_m(k\|k-1)=\mathbf{c}_m(k\|k-1)+h_{m,t}\mathbf{R}^{(t)}(k)$
	end if
10	$t=\arg\max_{j\in I_m^c}\frac{(\|c_{m,j}\|-\tau_m w_{m,j})^2}{R_{j,j}}$
	if $\|c_{m,t}\|>\tau_m w_{m,t}$
11	Include the t-th element into the support ($I_m\leftarrow I_m\cup t$)
	end if
12	⊛ Update the regularization parameter: $\tau_m\leftarrow\gamma\tau_m$
13	⊛ Approximately solve the equation (25) by using the LS-ℓ_1 optimization on the support I_m using the ℓ_1-DCD algorithm
14	⊛ Update the weight matrix $\mathbf{W}(k)$ using equation (34)
	end for
	end for

In a DCD iteration, the previously obtained solution $\hat{\mathbf{H}}(k-1)$ is used as a *warm-start* for minimizing the cost $\varepsilon'(k)$ at time k. This minimization is equivalent to minimization [52]

$$\frac{1}{2}\Delta\mathbf{H}(k)\mathbf{R}(k)\Delta\mathbf{H}^{\dagger}(k)-\Re\{\mathbf{C}(k|k-1)\Delta\mathbf{H}^{\dagger}(k)\}+\tau|\hat{\mathbf{H}}(k)|\mathbf{W}^{T}(k) \tag{35}$$

with respect to the matrix $\Delta\mathbf{H}(k)$, where $\mathbf{W}\in\mathbb{R}_{+}^{M\times L}$ is a weight matrix formed by reshaping the $ML\times 1$ vector $\mathbf{w}$, and $\mathbf{C}(k|k-1)$ is given by (30).

The cost function in (32) is minimized using the leading ℓ_1-DCD algorithm from [28]. In the leading ℓ_1-DCD algorithm, a criterion for terminating computations in every Homotopy iteration is a maximum number of DCD updates N_u. Typically, N_u is set to a small value for limiting the complexity of the algorithm [44].

Table I shows the EW-HRLS-DCD adaptive algorithm for time-varying MIMO channel estimation, where $\mathbf{c}_m(k|k-1)$ is the m-th row of the matrix $\mathbf{C}(k|k-1)$, $c_{m,j}$ is the j-th entry of the vector $\mathbf{c}_m(k|k-1)$, $h_{m,j}$ is the entry of channel matrix $\hat{\mathbf{H}}(k-1)$ in the m-th row and j-th column, $w_{m,j}$ is the entry of weight matrix $\mathbf{W}(k)$ in the m-th row and j-th column, and τ_m is the m-th element of vector $\boldsymbol{\tau}$.

IV. PROPOSED CE-BASED SOFT DECISION TURBO EQUALIZATION FOR MIMO SYSTEMS

In this section, we propose an iterative sparse channel estimation and equalization driven by the *a posteriori* soft-decision symbols for time-varying MIMO UWA communication system.

The proposed iterative receiver is shown in Fig. 3. It consists of the MIMO MMSE linear equalizer (LE), iterative MIMO adaptive channel estimator, soft-input soft-output (SISO) demappers, deinterleavers, SISO mappers, interleavers and MAP decoders. The iterative MIMO adaptive channel estimator provides an estimate of channel matrix, $\hat{\mathbf{H}}$, noise covariance vector $\hat{\boldsymbol{\sigma}}$ and phase vector $\hat{\boldsymbol{\theta}}$ driven by the training symbols $\mathbf{X}$, hard decision $Q(\hat{\mathbf{X}})$ and *a posteriori* soft decision $\tilde{\mathbf{X}}$; the phase vector $\hat{\boldsymbol{\theta}}$ is updated by an embedded second-order phase-locked loop (PLL) as used in [1], [45]. The MIMO TEQ applies a MMSE equalizer, and then hard or soft decisions of the equalized symbols are fed to the SISO demappers or the iterative MIMO adaptive channel estimator, respectively. The SISO demappers output the extrinsic information of the transmitted bits $\{L_e^E\{\mathbf{c}_n\}\}_{n=1}^{N}$, which is then passed to the de-interleavers and treated as the *a priori* information $\{L_a^D\{\mathbf{b}_n\}\}_{n=1}^{N}$ for the MAP decoder. Finally, the MAP decoders output extrinsic information $\{L_e^D\{\mathbf{b}_n\}\}_{n=1}^{N}$, which is further fed back to the equalizer as the *a priori* information $\{L_a^E\{\mathbf{c}_n\}\}_{n=1}^{N}$ of the transmitted bits. After several turbo iterations, the MAP decoders output estimates of transmitted bits $\{\mathbf{a}_n\}_{n=1}^{N}$.

A. Received Signal Model for MIMO Equalization

In the following, we assume the symbol rate sampling. Let $\mathcal{L}_f$ and $\mathcal{L}_p$ be the length of the noncausal and causal parts of the equalizer, respectively. In order to perform the equalization and estimate the transmitted symbols at time k, we consider an observation window containing $\mathcal{L}_p+\mathcal{L}_f+1$ received signal vectors, i.e., $\mathbf{y}(k-\mathcal{L}_p),\cdots,\mathbf{y}(k+\mathcal{L}_f)$. The received data can

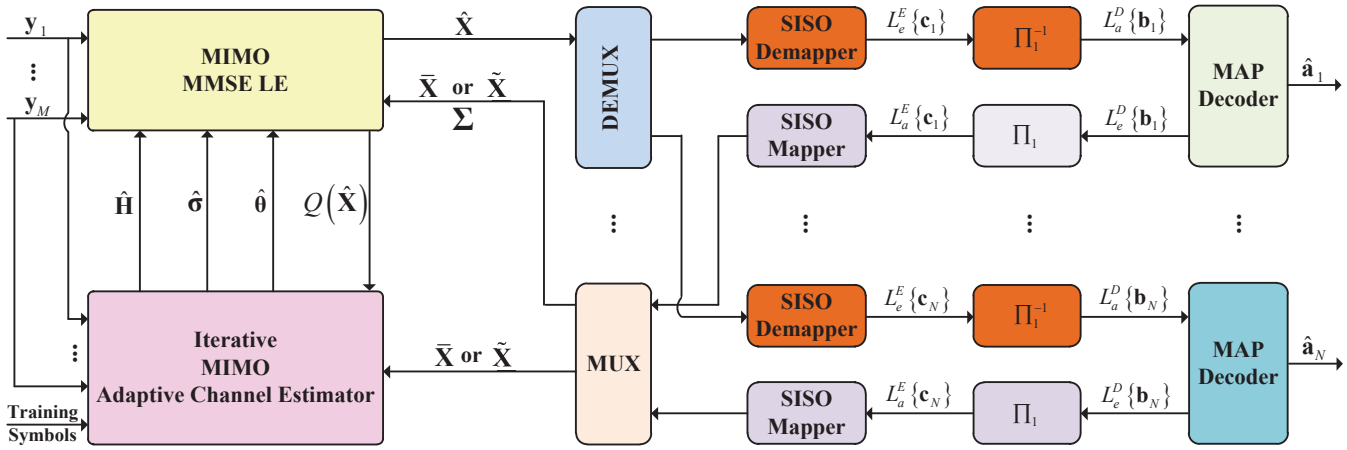

Fig. 3. Block diagram of iterative $N \times M$ MIMO receiver coupled with adaptive sparse channel estimator.

be written as [20], [56]

$$\mathbf{r}_k = \mathcal{H}_k \mathbf{s}_k + \mathbf{n}_k \tag{36}$$

where $\mathcal{H}_k$ is given by (37), shown at the bottom of the next page, and

$$\begin{aligned} \mathbf{r}_k &= \left[\mathbf{y}^T(k+\mathcal{L}_f), \cdots, \mathbf{y}^T(k-\mathcal{L}_p)\right]^T, && (38)\\ \mathbf{s}_k &= \left[\mathbf{x}^T(k+\mathcal{K}_f+\mathcal{L}_f), \cdots, \mathbf{x}^T(k-\mathcal{K}_p-\mathcal{L}_p)\right]^T && (39)\\ \mathbf{n}_k &= \left[\boldsymbol{\eta}^T(k+\mathcal{L}_f), \cdots, \boldsymbol{\eta}^T(k-\mathcal{L}_p)\right]^T. && (40) \end{aligned}$$

The channel length is $P = \mathcal{K}_p + \mathcal{K}_f + 1$, where $\mathcal{K}_f$ and $\mathcal{K}_p$ are the length of precursor and postcursor parts of the channel response, respectively. For convenience, we will denote $\mathcal{K} = N(\mathcal{K}_p + \mathcal{K}_f + \mathcal{L}_p + \mathcal{L}_f + 1)$ the overall length of the vector $\mathbf{s}_k$ and $\mathcal{L} = M(\mathcal{L}_p + \mathcal{L}_f + 1)$ the overall length of the vector $\mathbf{r}_k$. The noise vector $\mathbf{n}_k$ is assumed to be zero-mean complex Gaussian, i.e., $\mathbf{n}_k \sim \mathcal{CN}(\mathbf{0}, \sigma_{\mathbf{n}}^2 \mathbf{I}_{\mathcal{L}})$. The $\mathcal{H}_k$ is a block channel matrix made up of $\mathbf{H}_p(k)$ defined in (5), hence, the size of $\mathcal{H}_k$ becomes $\mathcal{L} \times \mathcal{K}$.

B. Linear MMSE Turbo Equalization

In practice, the channel impulse responses have to be estimated and then are used to calculate the coefficients of the TEQ. We denote $\hat{\mathcal{H}}_k$ and $\mathbf{E}_k = \mathcal{H}_k - \hat{\mathcal{H}}_k$ the channel estimate and the corresponding channel estimation error, respectively. Let us assume that $\mathbf{E}_k$ has zero mean and it is uncorrelated with $\hat{\mathcal{H}}_k$ and $\mathbf{s}_k$. Hence, we can rewrite (36) as $\mathbf{r}_k = \hat{\mathcal{H}}_k \mathbf{s}_k + (\mathbf{E}_k \mathbf{s}_k + \mathbf{n}_k)$. Given $\hat{\mathcal{H}}_k$, the linear MMSE estimate of $x_n(k)$ is obtained from [20], [38], [56]

$$\begin{aligned} \hat{\mathrm{x}}_n(k) &= \hat{\mathbf{f}}_n^{\dagger}(k)\left(\mathbf{r}_k - \hat{\mathcal{H}}_k \overline{\mathbf{s}}_n(k)\right), && (41)\\ \hat{\mathbf{f}}_n(k) &= \left(\hat{\mathcal{H}}_k \Sigma_{n,k} \hat{\mathcal{H}}_k^{\dagger} + \sigma_w^2 \mathbf{I}_{\mathcal{L}}\right)^{-1} \hat{\mathbf{h}}_n(k), && (42) \end{aligned}$$

where

$$\begin{aligned} \overline{\mathbf{s}}_n(k) &= \left[\overline{\mathbf{x}}^T(k+\mathcal{K}_f+\mathcal{L}_f), \cdots, \overline{\mathbf{x}}^T(k-1), \check{\mathbf{x}}_n^T(k), \right.\\ &\quad \left. \overline{\mathbf{x}}^T(k+1), \cdots, \overline{\mathbf{x}}^T(k-\mathcal{K}_p-\mathcal{L}_p)\right]^T, && (43)\\ \overline{\mathbf{x}}(k) &= [\bar{x}_1(k), \bar{x}_2(k), \cdots, \bar{x}_N(k)]^T, && (44)\\ \Sigma_{n,k} &= diag(v_{n,1}, \cdots, v_{n,k-1}, 1, v_{n,k+1}, \cdots, \\ &\quad v_{n,\mathcal{K}}), && (45)\\ \check{\mathbf{x}}_n(k) &= [\bar{x}_1(k), \cdots, \bar{x}_{n-1}(k), 0, \bar{x}_{n+1}(k), \cdots, \\ &\quad \bar{x}_N(k)]^T, && (46) \end{aligned}$$

and where $\overline{\mathbf{x}}(k)$ is *a priori* mean vector of $\mathbf{x}(k)$, and $\Sigma_{n,k}$ is the *a priori* covariance matrix of $\mathbf{x}(k)$. The vector $\hat{\mathbf{h}}_n(k)$ is the $(N(\mathcal{L}_p + P - 1) + n)$-th column of $\hat{\mathcal{H}}_k$. Hence, we can obtain $\bar{x}_n(k)$ and $v_{n,k}$ from *a priori* log-likelihood ratios (LLRs) as in [56]

$$\begin{aligned} \bar{x}_n(k) &\triangleq \mathrm{E}(x_n(k)) = \sum_{\alpha_i \in \mathcal{A}} \alpha_i \cdot P(x_n(k) = \alpha_i), && (47)\\ v_{n,k} &\triangleq \mathrm{Cov}(x_n(k), x_n(k)) = \left(\sum_{\alpha_i \in \mathcal{A}} |\alpha_i|^2 \cdot P(x_n(k) \right.\\ &\quad \left. = \alpha_i) \right) - |\bar{x}_n(k)|^2, && (48) \end{aligned}$$

where

$$\begin{aligned} P(x_n(k) = \alpha_i) &= \prod_{j=1}^{J} P(c_n^j(k) = s_{i,j}),\\ &= \prod_{j=1}^{J} 1/2 \cdot \big(1 \\ &\quad + \tilde{s}_{i,j} \cdot \tanh(L_a^E(c_n^j(k)/2))\big), && (49) \end{aligned}$$

the bit pattern $\mathbf{s}_i \triangleq [s_{i,1}, s_{i,2}, \cdots, s_{i,J}]$ corresponds to $\alpha_i \in \mathcal{A}$, and

$$\tilde{s}_{i,j} \triangleq \begin{cases} +1, s_{i,j} = 0 \\ -1, s_{i,j} = 1 \end{cases}. \tag{50}$$

The extrinsic LLR for $c_n^j(k)$ is given by (51), shown at the bottom of the next page, where $\hat{\mu}_n(k) = \hat{\mathbf{f}}_n^H(k) \hat{\mathbf{h}}_n(k)$, and $\mathcal{A}_j^0$ and $\mathcal{A}_j^1$ are the set of all constellation points such that $s_{i,j}$ is 0 and 1, respectively [56].

C. A Posteriori Soft Decision

After first equalization, the *a posteriori* soft decision $\tilde{x}_n(k)$ of the equalized symbol $\hat{x}_n(k)$ is available and can be calculated as [27], [37]

$$\tilde{x}_n(k) = \sum_{\alpha_i \in \mathcal{A}} \alpha_i P\Big(x_n(k) = \alpha_i | \hat{x}_n(k)\Big) \tag{52}$$

where $P\Big(x_n(k) = \alpha_i | \hat{x}_n(k)\Big)$ is the *a posteriori* probability of $x_n(k)$ and is given by (53), shown at the bottom of the next page. $P\left(x_n(k) = \alpha_i\right)$ is the *a priori* probability and can be calculated with the *a priori* LLRs from the MAP decoder as in (49), and $p\left(\hat{x}_n(k)\right)$ is computed with the normalization $\sum_{i=1}^{2^q} P\Big(x_n(k) = \alpha_i | \hat{x}_n(k)\Big) = 1$. Under the assumption of the Gaussian distribution as in [56], the equalizer output $\hat{x}_n(k)$ conditioned on $x_n(k) = \alpha_i$ is given by:

$$p\left(\hat{x}_n(k) | x_n(k) = \alpha_i\right) = \frac{1}{\pi \tilde{\delta}_n^2} \exp\left\{ -\frac{|\hat{x}_n(k) - \tilde{x}_n(k)\alpha_i|^2}{\tilde{\delta}_n^2} \right\}, \tag{54}$$

where the *a posteriori* variance of $x_n(k)$ is obtained as

$$\tilde{\delta}_n^2 = \sum_{i=1}^{2^Q} |\alpha_i - \tilde{x}_n(k)|^2 P\Big(x_n(k) = \alpha_i | \hat{x}_n(k)\Big). \tag{55}$$

Over the turbo iterations, the reliability of the *a posteriori* soft decision $\tilde{x}_n(k)$ increases thus improving the accuracy of channel estimation and also speeding up the convergence of the channel estimator.

D. A Posteriori Soft Decision Driven Homotopy RLS-DCD Algorithm

In the iterative channel estimation based on adaptive filtering, the adaptive filter is driven by the decision error $\boldsymbol{e}(k)$. The adaptive channel estimation algorithm aims to minimize the variance of the decision errors, so the reliability of the decision plays a very important role in the adaptive channel estimation. In practice, the adaptive channel estimator generally works under two modes: the training mode and direct-decision mode. According to the mode, we can define three types of decision error as following [58]

$$\boldsymbol{e}(k) = \mathbf{y}(k) - \hat{\mathbf{H}}(k-1)\boldsymbol{\chi}(k) \in \mathbb{C}^{M\times 1}, \tag{56}$$

$$\hat{\boldsymbol{e}}(k) = \mathbf{y}(k) - \hat{\mathbf{H}}(k-1)Q(\hat{\boldsymbol{\chi}}(k)) \in \mathbb{C}^{M\times 1}, \tag{57}$$

$$\bar{\boldsymbol{e}}(k) = \mathbf{y}(k) - \hat{\mathbf{H}}(k-1)\bar{\boldsymbol{\chi}}(k) \in \mathbb{C}^{M\times 1}, \tag{58}$$

where $\boldsymbol{\chi}(k)$ presents the perfect decision corresponding to the training mode. The vector $\bar{\boldsymbol{\chi}}(k)$ consists of *a priori* soft decisions of transmitted symbols under the direct-decision mode, and $Q(\hat{\boldsymbol{\chi}}(k))$ denotes the hard decision of the equalizer output, $\hat{\boldsymbol{\chi}}(k)$. In what follows, the vectors $\boldsymbol{e}(k)$, $\bar{\boldsymbol{e}}(k)$ and $\hat{\boldsymbol{e}}(k)$ are named the perfect decision error vector, *a priori* soft decision error vector and hard decision error vector, respectively.

In existing iterative adaptive channel estimation algorithms, the hard decision or *a priori* soft decision symbols are used for driving the estimator. In [27], [37], an efficient adaptive turbo equalizer is proposed, where the more reliable *a posteriori* soft decisions are used in the adaptive update of the channel coefficients and for the MMSE equalizer. In order to reduce the complexity of the adaptive turbo equalization, the equalizer filter coefficients are adaptively updated via the normalized LMS (NLMS) [39] or the IPNLMS [24] algorithm. The DA-TEQ scheme with the *a posteriori* soft decisions achieves faster convergence and higher spectrum efficiency than schemes with hard decision or with *a priori* soft decision. Inspired by [37], here, we use the *a posteriori* soft decisions to drive the channel estimator. For convenience, we define the *a posteriori* decision error vector as

$$\tilde{\boldsymbol{e}}(k) = \mathbf{y}(k) - \hat{\mathbf{H}}(k-1)\tilde{\boldsymbol{\chi}}(k) \in \mathbb{C}^{M\times 1} \tag{59}$$

where $\tilde{\boldsymbol{\chi}}(k)$ is the *a posteriori* soft decision vector of the equalizer output $\hat{\boldsymbol{\chi}}(k)$.

The proposed iterative channel estimator comprises the following two stages:

1) Training Stage: The known training symbols $x_n(k)$ within the training symbol vector $\boldsymbol{\chi}(k)$ are used to estimate the channel impulse response.

2) Direct-Decision Stage: There are no known training symbols available at this stage. The hard-decisions of the equalizer output $\hat{x}_n(k)$ are usually used for tracking the channel. However, the hard-decision is not reliable, leading to error decisions on the transmitted symbols. Hence, the decision errors will cause the error propagation, which can be catastrophic for turbo equalization. Iterative channel estimators in turbo equalization schemes mostly employ the hard-decision or *a priori* soft decisions at the direct-decision stage. At the initial stage of turbo equalization, the *a priori* or *a posteriori* soft-decision from the decoder or equalizer is not yet available, thus we use hard-decisions of the equalizer output as training symbols for the channel estimation. In subsequent iterations, the *a posteriori* soft decisions, which possess higher reliability than the *a priori* soft decisions, are utilized.

$$\mathcal{H}_k = \begin{bmatrix} \mathbf{H}_{p-\mathcal{K}_f}(k+\mathcal{L}_f) & \cdots & \mathbf{H}_{p-\mathcal{K}_p}(k+\mathcal{L}_p) & \mathbf{0} & \mathbf{0} \\ \mathbf{0} & \ddots & \cdots & \ddots & \mathbf{0} \\ \mathbf{0} & \mathbf{0} & \mathbf{H}_{p+\mathcal{K}_f}(k-\mathcal{L}_p) & \cdots & \mathbf{H}_{p+\mathcal{K}_p}(k-\mathcal{L}_p) \end{bmatrix}, \tag{37}$$

$$L_{\mathrm{e}}^E\left(c_n^j(k)\right) = \ln \frac{\sum_{\theta\in\mathcal{A}_j^0} \exp\left(-\frac{|\hat{x}_n(k) - \hat{\mu}_n(k)\theta|^2}{\hat{\mu}_n(k)(1-\hat{\mu}_n(k))} + \frac{1}{2}\sum_{i=1,i\neq j}^{J} \tilde{s}_{i,j} L_a^E(c_n^i(k)) \right)}{\sum_{\theta\in\mathcal{A}_j^1} \exp\left(-\frac{|\hat{x}_n(k) - \hat{\mu}_n(k)\theta|^2}{\hat{\mu}_n(k)(1-\hat{\mu}_n(k))} + \frac{1}{2}\sum_{i=1,i\neq j}^{J} \tilde{s}_{i,j} L_a^E(c_n^i(k)) \right)} \tag{51}$$

E. A Posteriori Soft Decision Driven Turbo Equalization

The quality of the soft decision plays a very important role in the performance of the MMSE equalizer. The *a priori* soft decisions are adopted in many adaptive turbo equalization schemes [21], [22], [57]. With the more reliable *a posteriori* soft decisions, performance of MMSE equalizer can be improved [37]. The output of *a posteriori* soft decision driven equalizer, $\hat{x}_n(k)$, is obtained as

$$\hat{\mathrm{x}}_n(k) = \hat{\mathbf{f}}_n^H(k)\left(\mathbf{r}_k - \hat{\mathcal{H}}_k\tilde{\mathbf{s}}_n(k)\right) \tag{60}$$

Here, we utilized the *a posteriori* soft decisions $\tilde{\mathbf{s}}_n(k) = \left[\tilde{\mathbf{x}}^T(k+\mathcal{K}_f+\mathcal{L}_f),\cdots,\tilde{\mathbf{x}}^T(k-1),\vec{\mathbf{x}}_n^T(k),\tilde{\mathbf{x}}^T(k+1),\cdots,\tilde{\mathbf{x}}^T(k-\mathcal{K}_p-\mathcal{L}_p)\right]^T$ instead of the *a priori* soft decisions $\bar{\mathbf{s}}_{n,k}$ in (41), where $\tilde{\mathbf{x}}(k) = [\tilde{x}_1(k),\tilde{x}_2(k),\cdots,\tilde{x}_N(k)]^T$ when $k^{'} \neq k$ for $k^{'} \in [k-\mathcal{K}_p-\mathcal{L}_p, k+\mathcal{K}_f+\mathcal{L}_f]$, and $\vec{\mathbf{x}}_n(k) = [\tilde{x}_1(k),\cdots,\tilde{x}_{n-1}(k),0,\tilde{x}_{n+1}(k),\cdots,\tilde{x}_N(k)]^T$ when $k^{'} = k$; obviously, $\tilde{x}_n(k)$ is excluded for avoiding self cancellation [37].

V. Complexity Comparison for MIMO Channel Estimators

In this section, the complexity of two channel estimators, EW-RLS and EW-HRLS-DCD, is compared. The algorithm complexity is evaluated in terms of the number of real-valued multiplications, additions, square-root, and division operations per time sample.

The work [28] details the complexity of the EW-HRLS-DCD algorithm for SISO system. According to the general structure of adaptive MIMO channel estimator as shown in Fig. 2, the $N \times M$ MIMO system can be treated as M SISO systems with a channel length of $L = NP$ each. Hence, the complexity of the EW-HRLS-DCD algorithm for MIMO system can be easily calculated by following steps in [28] for a SISO system. We can approximately estimate the complexity of the channel estimator based on the EW-HRLS-DCD algorithm for a MIMO system as presented in Table II.

In Table I, step 13 requires using the leading ℓ_1-DCD algorithm, where M_b is the number of bits used for representation of entries in the solution vector, this defining the accuracy of the fixed-point representation [44], and N_u is a maximum number of DCD iterations. The update of the vector $\mathbf{c}_m(k|k-1)$ in the leading ℓ_1-DCD algorithm is the most consuming part of the algorithm. The details of the involving computation of the leading ℓ_1-DCD algorithm are found in Table II in [28], and the reader is referred to detail [52].

In overall, as shown in Table II, the EW-HRLS-DCD algorithm requires about $32MNP+5M|I|+2M|I|(M_b+N_u)$ real-valued multiplications, $25MNP+2M|I|+2M|I|(M_b+N_u)$ real-valued additions, $M(1+NP)+M(M_b+N_b)$ square-root operations, and $2MNP-M|I|$ real-valued divisions.

For comparison, arithmetic operations in the conventional EW-RLS algorithm described by equations (16)-(19) are listed in Table III. The overall complexity of the conventional EW-RLS algorithm roughly requires $12(NP)^2+8MNP$ real-valued multiplications, $9(NP)^2+6MNP+M$ real-valued additions, and $(2M+2NP+1)NP$ real-valued divisions.

For first example, for $N=2$, $M=8$, $P=40$, $K=6$, $N_u=4$, $M_b=15$, and assuming that $|I|=K$, we obtain that the EW-HRLS-DCD algorithm from [52] requires about 23×10^3 multiplications, 18×10^3 additions, 800 square-root operations, and 1.2×10^3 divisions per time index. The same figures for the EW-RLS algorithm are 80×10^3, 61×10^3, 0, and 14×10^3, respectively. Thus, compared to the EW-RLS algorithm, the EW-HRLS-DCD algorithm reduces the number of multiplications by about 3.5 times, the number of additions by about 3.4 times, and the number of divisions by about 11 times.

For another example with the parameter setup the same as in the first example except for the length of channel P, which is now $P=100$, the EW-HRLS-DCD algorithm requires about 53×10^3 multiplications, 42×10^3 additions, 1.8×10^3 square-root operations, and 3.2×10^3 divisions per time index. The same figures for the EW-RLS algorithm are 490×10^3, 370×10^3, 0, and 83×10^3, respectively. Thus, compared to the EW-RLS algorithm, the EW-HRLS-DCD algorithm reduces the number of multiplications by about 9 times, the number of additions by about 9 times, and the number of divisions by about 26 times.

VI. Experimental Results

In this section, we evaluate the performance of a receiver with the proposed soft-decision-driven sparse channel estimation and turbo equalization scheme and compare it to other receivers.

A. Experimental Environment

The experiment was conducted in the Songhua Lake, Jilin province, China (SHLake2013) on Nov. 2013. The lake depth at the experimental site is 48.6 m. Two transducers (antennas) were deployed off a small boat and submerged at about 5 m and 6 m below the surface, respectively. During the experiment, the small boat was drifting with an approximate maximum speed of 0.25 m/s. The receive vertical linear array of 48 hydrophones was moored with the first hydrophone (closest to the lake bottom) at about 7 m above the lake bottom, and other hydrophones evenly spaced by 0.25 m. The communication range was about 2.1 km at the start of the experiment.

B. Signaling and Data Structure

For MIMO transmission, two concurrent data streams with the BICM horizontal encoding scheme were transmitted by using two transducers. The input bits were encoded by a

$$P\left(x_n(k)=\alpha_i|\hat{x}_n(k)\right) = \frac{p(\hat{x}_n(k)|x_n(k)=\alpha_i)}{p(\hat{x}_n(k))}P(x_n(k)=\alpha_i). \tag{53}$$

TABLE II
COMPUTATIONAL COMPLEXITY OF THE EW-HRLS-DCD CHANNEL ESTIMATOR

Step	Multiplications ($\times$)	Additions ($+$)	Square-roots ($\sqrt{\cdot}$)	Divisions ($\div$)
1	$6MNP$	$4MNP$	–	–
2	$4MNP$	$4MNP$	–	–
3	$4MNP$	$4MNP$	–	–
5	$6MNP$	$4MNP$	–	–
7	$2MNP$	$2MNP$	M	–
9	$M(4NP+7\|I\|)$	$M(2NP+4\|I\|)$	$M\|I\|$	–
11	$2M(NP-\|I\|)$	$2M(NP-\|I\|)$	$M(NP-\|I\|)$	$M(NP-\|I\|)$
13	$2M\|I\|(M_b+N_u)$	$2M\|I\|(M_b+N_u)$	$M(M_b+N_u)$	–
14	$4MNP$	$3MNP$	–	MNP
Total	$32MNP+5M\|I\|$ $+2M\|I\|(M_b+N_u)$	$25MNP+2M\|I\|$ $+2M\|I\|(M_b+N_u)$	$M(1+NP)$ $+M(M_b+N_b)$	$2MNP-M\|I\|$

TABLE III
COMPUTATIONAL COMPLEXITY OF THE EW-RLS CHANNEL ESTIMATOR

Equation	Multiplications ($\times$)	Additions ($+$)	Square-roots ($\sqrt{\cdot}$)	Divisions ($\div$)
(15)	$4(NP)^2$	$3(NP)^2$	–	NP
(16)	$4MNP$	$3MNP+M$	–	–
(17)	$8(NP)^2$	$6(NP)^2$	–	$2(NP)^2$
(18)	$4MNP$	$3MNP$	–	$2MNP$
Total	$12(NP)^2+8MNP$	$9(NP)^2+6MNP+M$	–	$(2M+2NP+1)NP$

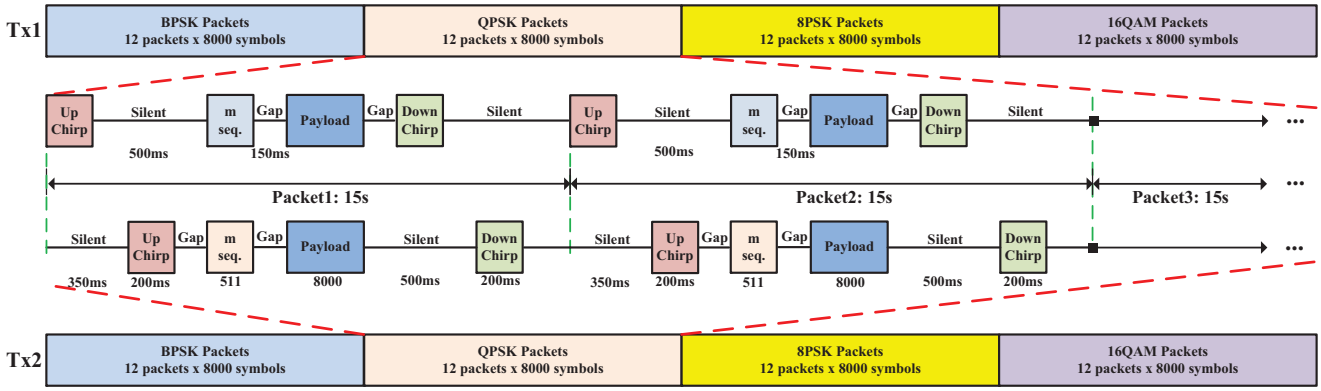

Fig. 4. The structure of the data streams in a two-transducer transmission in the SHLake2013 experiment.

rate $R_c = 1/2$ convolutional coder with generator polynomial [171, 133] in octal format. The carrier frequency was $f_c = 3\ kHz$ and the symbol rate was 2 k symbols per second ($ksps$). The pulse shaping filter was a square-root raised cosine filter with a roll-off factor of 0.2 [40], leading to an occupied channel bandwidth of about 2.4 kHz. The sampling rate was 25 kHz at the receiver end.

The data structure of the two data streams and relevant parameters are shown in Fig. 4. Preamble up-chirp and postamble down-chirp, Doppler-insensitive waveforms, were added before and after the data burst for coarse frame synchronization and estimation of an average Doppler shift over the whole data burst. In order to reduce the co-channel interference, two Gold sequences of length 511, Doppler-sensitive waveforms, generated from preferred pairs of m-sequences [40] and added before and after the data payload were used for coarse frame synchronization and initial estimation of channel parameters [40]. Following the frame synchronization signal is one data packet (payload) with various modulation formats. Only data with QPSK, 8PSK and 16QAM modulations are used for performance evaluation, since the detection performance is very good with the BPSK modulation. The payload is separated from the m-sequence and up-chirp or down-chirp signal by the gap with the duration 150 ms for avoiding the inter-block interference. The length of each payload is 8000 symbols between two gaps. Each burst packet is transmitted every 15 s. The entire duration of data transmission is 12 minutes. The approximate SNR, which is estimated by using the signal part and silent part of received signal, is in the range of 20 dB to 32 dB.

In order to show characteristics of the UWA channel during the experiment, we use the conventional EW-RLS algorithm to estimate the channel impulse response (CIR) over 8000 symbols with QPSK modulation as an example. In Fig. 5, the CIR between the first transducer and last hydrophone (near the surface) is shown in Fig. 5(a). Fig. 5(b) shows the CIR between the second transducer and last hydrophone estimated by using the matched filter applied to the preamble and postamble chirp signals. In Fig. 5, we can observe that the channel multipath spread is about $16 \sim 20\ ms$, corresponding to a channel length of $32 \sim 40$ taps in terms of the symbol rate $R_s = 2\ ksps$. There are three clusters with high energy in the delay domain.

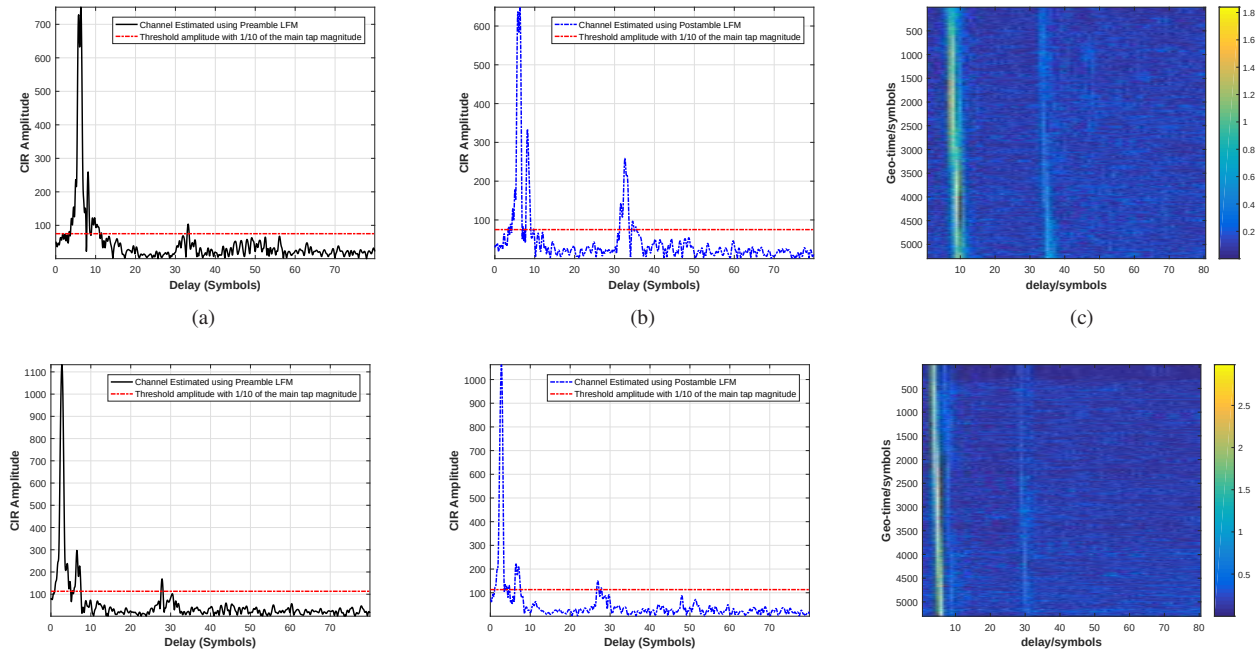

Fig. 5. Examples of the CIR estimated over one burst transmission. The CIRs measured between the first transducer and last hydrophone are shown on the top row. The CIRs measured between the second transducer and last hydrophone are shown on the bottom row. CIR is measured using: (a) and (d) the preamble up-chirp with the correlation method; (b) and (e) the postamble down-chirp with the correlation method; (c) and (f) data signals and the classical EW-RLS algorithm with $\lambda = 0.997$.

The arrival paths fluctuate very rapidly. It is important to notice that the channel impulse response is sparse.

C. Performance versus the Training Overhead

In order to investigate the convergence performance of channel estimators based on the soft decisions, we only consider 2×4 MIMO configuration, as an example. Firstly, we divide the whole hydrophone array into sub-arrays with four hydrophones. In this sub-section, we consider the separation of the 2×48 MIMO system into twelve 2×4 MIMO systems, so for each modulation format and 12 transmitted packets we can equivalently obtain 144 received bursts. Secondly, training symbols are periodically inserted into the data to estimate the fast time-varying channel. The whole payload is divided into eight sub-blocks with $N_s = 1000$ symbols in each. For each sub-block, the first N_p symbols are utilized as the training symbols and the remaining $N_d = N_s - N_p$ data symbols. The resulting training overhead is $\beta = N_p/(N_p + N_d)$, and the corresponding data rate is $(1 - \beta) \times R_s JNR_c \ kbps$. The choice of N_p depends on the modulation scheme as shown in Table IV. Table IV lists two configurations with two training overheads each. To ensure a fair comparison between all adaptive channel estimators, the parameters for each estimator are optimized by exhaustive search so that the lowest possible BER is achieved. In order to reduce the dimension of the exhaustive search, some parameters for the MIMO turbo linear equalizer are fixed; more specifically, $\mathcal{K}_p$, $\mathcal{K}_f$, $\mathcal{L}_p$ and $\mathcal{L}_f$ are set to 80, 40, 40, and 40, respectively. These parameters can be estimated using the preamble and postamble chirp signals. The convergence speed of the NLMS-type algorithms is much slower than that of the RLS-type algorithms, therefore, to improve the performance, the data reuse technique is used in the IPNLMS channel estimator configured as in [23], [37], [38]. The detection performance is measured based on the number of data packets achieving a specific BER level. Table V and Table VI show the summary of the results for configuration C1 and configuration C2, respectively. The performance of iterative channel estimation based on the IPNLMS [38] and conventional EW-RLS is also included. We can observe the following results from Table V: 1) the performance of all schemes is improved with iterations. However TEQs based on RLS-type algorithms outperform the TEQ based on the IPNLMS even after the first iteration. The performance gap between TEQs based on RLS-type algorithms and IPNLMS is further increased for the 8PSK and 16QAM modulation schemes due to more accurate channel estimates obtained by the RLS-type based channel estimators; 2) the performance improvement is significant at the first, second and third iterations; 3) the TEQ based on the EW-HRLS-DCD algorithm outperforms the TEQ based on the EW-RLS algorithm.

Next, we consider how the detection performance of the TEQs is affected by the training overhead. Firstly, the similar trends in behavior of the TEQs between configurations C1 and C2 can be observed, but the increase in the training overhead improves the performance of all the three TEQs. We observe that the TEQ based on the IPNLMS algorithm is particularly sensitive to the training overhead. A considerable performance gain is achieved after the first iteration for all three modulation formats. On the other hand, after five iterations the improvement for the IPNLMS algorithm is small due to the slow convergence and limited by the fast time-varying channel

TABLE IV
RECEIVER CONFIGURATIONS FOR THE ANALYSIS OF CONVERGENCE PERFORMANCE

Configuration	Modulation	Packets	Sub-block (N_s)	Training overhead (β)	Data rate ($kbps$)
C1	QPSK	144	1000	20%	3.2
	8PSK	144	1000	20%	4.8
	16QAM	144	1000	30%	5.6
C2	QPSK	144	1000	30%	2.8
	8PSK	144	1000	30%	4.2
	16QAM	144	1000	35%	5.2

TABLE V
TOTAL NUMBER OF PACKETS ACHIEVING THE SPECIFIED BER LEVEL FOR CONFIGURATION C1

# of Iter.	QPSK (BER = 0)			8PSK (BER $\in [0, 10^{-4}]$)			16QAM (BER $\in [0, 10^{-3}]$)		
	IPNLMS	RLS	HRLS-DCD	IPNLMS	RLS	HRLS-DCD	IPNLMS	RLS	HRLS-DCD
0	0	0	0	0	0	0	0	0	0
1	27	63	83	3	13	52	1	16	42
2	68	98	110	8	39	87	2	33	71
3	83	105	134	10	42	97	4	43	84
4	83	105	134	13	50	104	5	47	92
5	86	108	136	14	51	108	6	47	92

TABLE VI
TOTAL NUMBER OF PACKETS ACHIEVING THE SPECIFIED BER LEVEL FOR CONFIGURATION C2

# of Iter.	QPSK (BER = 0)			8PSK (BER $\in [0, 10^{-4}]$)			16QAM (BER $\in [0, 10^{-3}]$)		
	IPNLMS	RLS	HRLS-DCD	IPNLMS	RLS	HRLS-DCD	IPNLMS	RLS	HRLS-DCD
0	0	0	0	0	0	0	0	0	0
1	60	79	124	7	35	71	14	31	60
2	84	92	132	14	57	105	21	46	80
3	90	105	132	18	64	120	23	50	84
4	96	113	141	20	71	122	25	50	93
5	97	113	141	20	72	123	26	51	93

(i.e. shorter channel coherence time). For example, the final number of the packets with zero BER increases from 86 to 97 after five iterations for the QPSK modulation. With the RLS-type based channel estimators for all modulation formats as shown in Table VI, there is some increase in the number of packets that achieve the target BER by increasing the number of training symbols.

Fig. 6 details the demodulation results. As shown in the figure, the EW-HRLS-DCD based TEQ can successfully retrieve the 141 data packets out of 144 packets for the QPSK modulation. This implies that our proposed receiver can achieve a data rate of 3.2 $kbps$ with a low error probability. On the other hand, for the 8PSK case, with our receiver and 20% training overhead, there are 122 packets with BER $< 10^{-4}$, there are 137 packets with BER $< 10^{-4}$ when 30% training overhead is used. Note that for the 16QAM modulation, the large performance gain can be observed in terms of the total number of the packets with BER $< 10^{-2}$.

The constellation diagram is a useful tool to demonstrate the reliability of the received and equalized symbols. The evolutional behavior of the equalized and *a posteriori* soft-decision symbols in terms of constellation diagram are shown in Fig. 7 and Fig. 8, respectively. Results for the 16QAM modulation in the four iterations are only presented. In Fig. 7, for the channel estimator based on the IPNLMS algorithm, the improvement in the quality of the equalized symbols with iterations is little, while the improvement in quality obtained by RLS-type channel estimators is more considerable. On the other hand, compared to the RLS channel estimator, the EW-HRLS-DCD channel estimator can achieve better quality of equalized symbols with more iterations.

Fig. 8 shows the evolution of the *a posteriori* soft-decision symbols. What is interesting to observe is that the soft-decision symbols in all the three schemes can almost converge to the ideal constellation points. For schemes based on RLS and EW-HRLS-DCD channel estimators, these results are consistent with the results shown in Fig. 7(b) and Fig. 7(c). From Fig. 7(a), it is however difficult to recognize the modulation scheme even after five iterations. Obviously, the result shown in Fig. 8(a) is a counterintuitive from the observation in Fig. 7(a). This appears due to inaccurate channel estimation provided by the IPNLMS algorithm, which is catastrophic for turbo equalization. The *a posteriori* soft-decision evaluated from the equalizer based on the IPNLMS channel estimator converges to the wrong constellation points due to the error propagation incurred by inaccurate channel estimates. With a high quality of channel estimation as shown in Fig. 8(b) and Fig. 8(c), the *a posteriori* soft-decision symbols are more reliable than equalized symbols due to accurate channel estimates and the usage of the soft decoder. However, with inaccurate channel estimates, the *a posteriori* soft-decision symbols convergence to wrong constellation points due to the error propagation in turbo iteration procedure as shown in Fig. 8(a).

D. Performance versus MIMO size

Table VII shows three configurations of MIMO system used to demonstrate the effect of the MIMO size on the

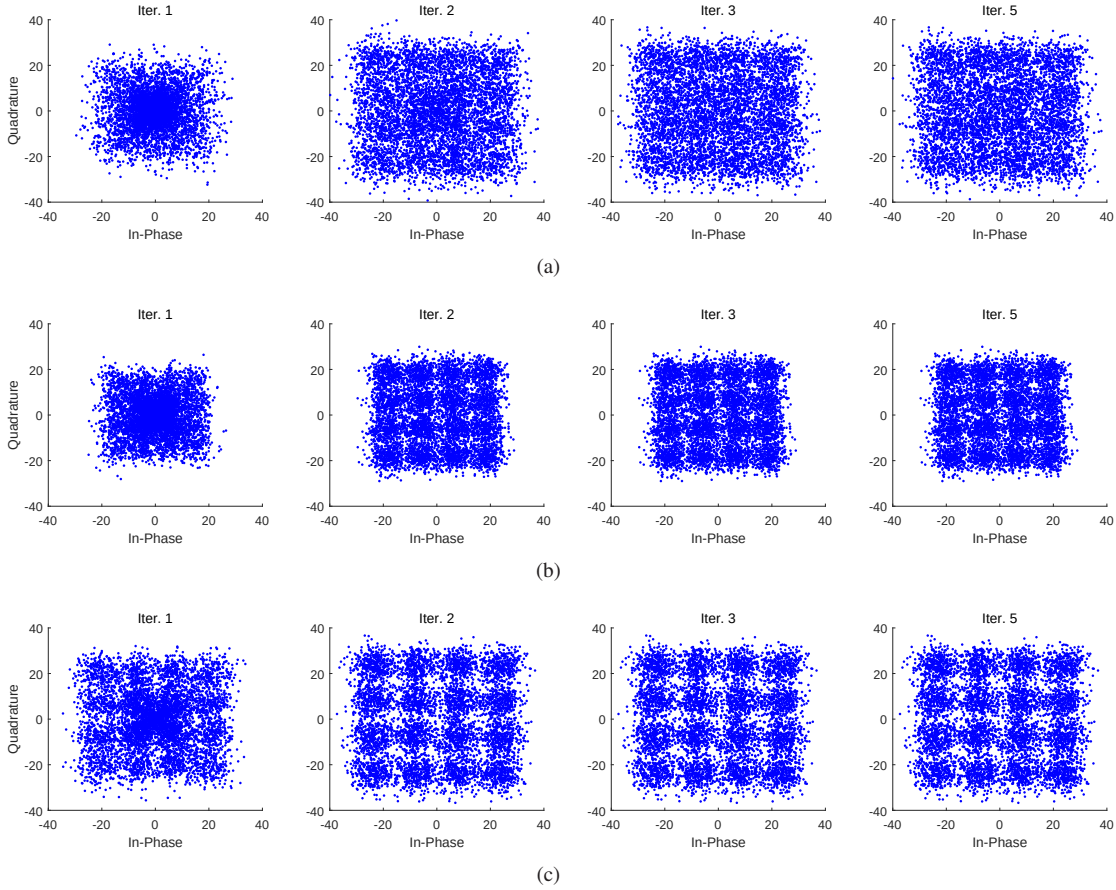

Fig. 7. Constellation diagrams of the equalized symbols for one burst. Five iterations are conducted with the iterative channel estimation algorithm: (a) IPNLMS; (b) RLS; (c) EW-HRLS-DCD.

TABLE VII
RECEIVER CONFIGURATIONS FOR THE ANALYSIS OF CONVERGENCE PERFORMANCE

MIMO ($N \times M$)	Modulation	Packets	Sub-block (N_s)	Training overhead (β)	Data rate ($kbps$)
2×4	QPSK	144	1000	20%	3.2
	8PSK			20%	4.8
	16QAM			30%	5.6
2×8	QPSK	72	1000	20%	3.2
	8PSK			20%	4.8
	16QAM			30%	5.6
2×12	QPSK	48	1000	20%	3.2
	8PSK			20%	4.8
	16QAM			30%	5.6

receiver performance. The 2×48 MIMO system is grouped into multiple smaller MIMO systems according to the number of hydrophones, leading to 144, 72 and 48 received packets for the 2×4, 2×8 and 2×12 MIMO setups, respectively.

In Fig. 9 it can be seen that with the QPSK modulation, all the MIMO receivers can achieve perfect data recovery with eight or twelve hydrophones after five turbo iterations.

For the 8PSK modulation, the IPNLMS-based MIMO receiver improves the performance with more hydrophones, but it cannot achieve the zero BER performance. The main reason is that the demodulation for a higher modulation order requires a higher accuracy of channel estimation, which cannot be provided by the IPNLMS algorithm. However, the zero-BER detection is achieved by MIMO receivers with both RLS- and EW-HRLS-DCD-based channel estimators, in the 2×12 configuration.

In Fig. 9(c), detection results are shown for the 16QAM modulation. Generally, the performance of all channel estimators keeps improving with more hydrophones. For the 2×8 MIMO setup, 2, 8 and 12 error free packets of 72 packets are received with IPNLMS, RLS and EW-HRLS-DCD based receiver, respectively. There are 36, 59 and 64 data packets out of 72 packets with BER $< 10^{-2}$ for these estimators, respectively. With the 2×12 MIMO configuration, there are 33, 46 and 48 data packets out of 48 packets with BER $< 10^{-2}$ for the three estimators, respectively.

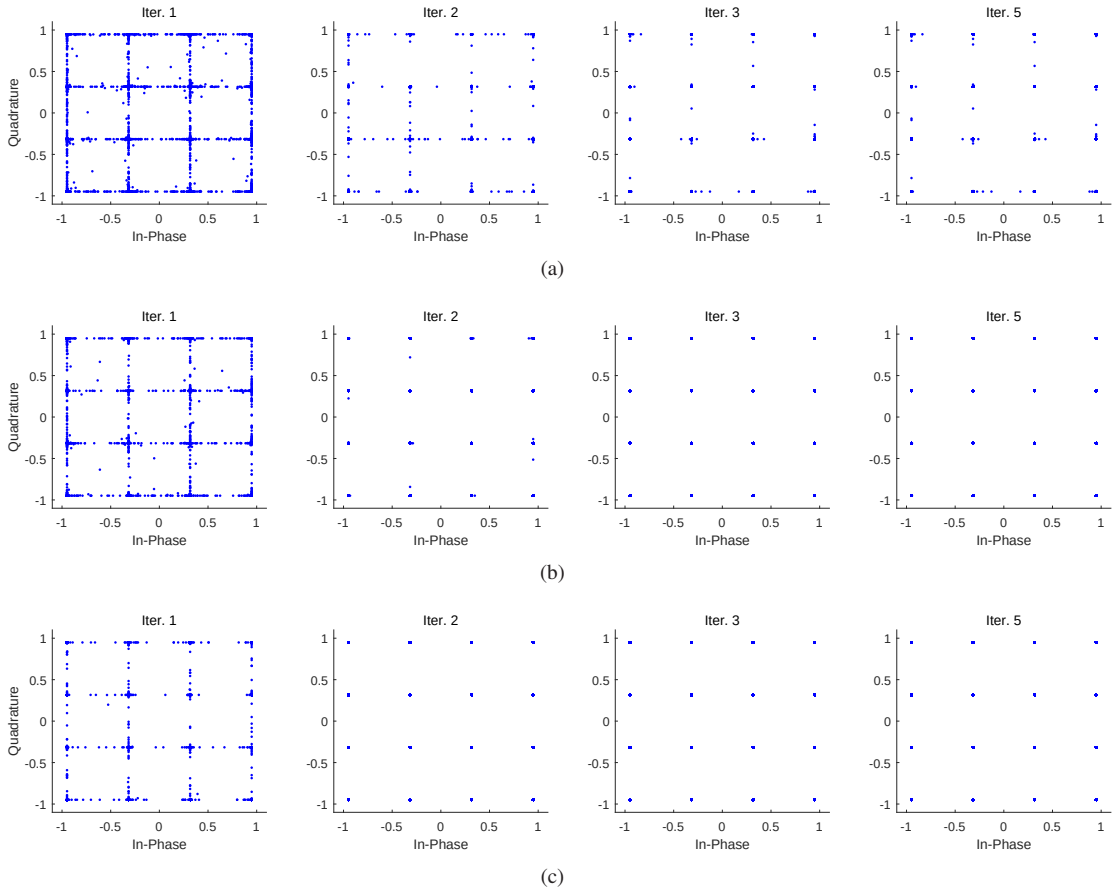

Fig. 8. Constellation diagrams of the *a posteriori* soft-decision symbols for one burst. Five iterations are conducted with the iterative channel estimation algorithm: (a) IPNLMS; (b) RLS; (c) EW-HRLS-DCD.

E. Comparison between Hard-decision and Soft-decision driven Turbo Equalization

As shown in many research works [20], [23], [31], [37], [38], [57], [58], the quality of the output of turbo equalizer with high order modulation is very sensitive to the channel estimation errors or misadjustment errors produced by a specific adaptive algorithm. On the other hand, the hard decision of the equalizer output detriments the quality of channel estimation and MMSE equalizer due to the error propagation.

Since the true CIRs are not known for the experimental data processing, we can not evaluate the accuracy of channel estimation with various feedback information in terms of MSE. In order to quantify the performance gain brought by channel estimators with different feedback, in [21], the behavior of turbo receiver was investigated in terms of decision-directed mean squared error (DD-MSE) at the output of equalizer versus the number of iterations. The DD-MSE can be estimated adaptively as follows [21], [37]:

$$\varepsilon_{MSE}^{k+1} = \gamma \varepsilon_{MSE}^{k} + (1-\gamma)|e_k|^2, \tag{61}$$

where the forgetting factor γ is set to 0.99. The error e_k can be replaced by $\hat{e}(k)$, $\bar{e}(k)$, or $\tilde{e}(k)$ corresponding to the hard decision error, *a priori* soft decision error, or *a posteriori* soft decision error defined as in (57), (58) and (59), respectively. It is noted that e_k is replaced by the hard decision error due to unavailable *a priori* information from decoder at the initial turbo iteration.

From the analysis in the previous subsections, with a small MIMO size, the TEQs based on the IPNLMS algorithm experience problems for high order modulation due to the error propagation. Therefore, the comparison between the proposed TEQ and the hard decision based TEQ is limited to the 2×8 MIMO with 8PSK modulation. In addition, we only choose those packets, which do not experience convergence problem by using all the three channel estimators, for fair benchmark in following analysis.

Fig. 10 depicts the DD-MSE for the three channel estimators and for the hard-decision and *a posteriori* SD feedback. Clearly, for all the estimators, the TEQ with the *a posteriori* SD outperforms that with the hard-decisions. With the *a posteriori* SD, the IPNLMS based channel estimator approximately obtains $4\ dB$ DD-MSE gain, the RLS based channel estimator approximately obtains $7\ dB$ DD-MSE gain, the EW-HRLS-DCD based channel estimator approximately obtains $7\ dB$ DD-MSE gain with respect to that with the hard-decision feedback. On the other hand, comparison of the three channel estimators shows that the smallest DD-MSE is achieved by the EW-HRLS-DCD algorithm with the *a posteriori* SD.

Finally, Fig. 11 demonstrates the performance of TEQs with three channel estimators versus the number of turbo

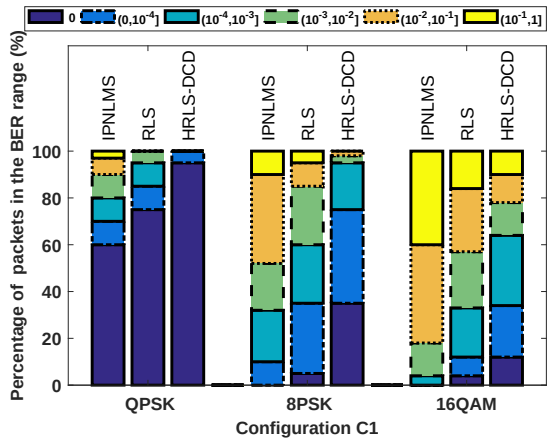

(a)

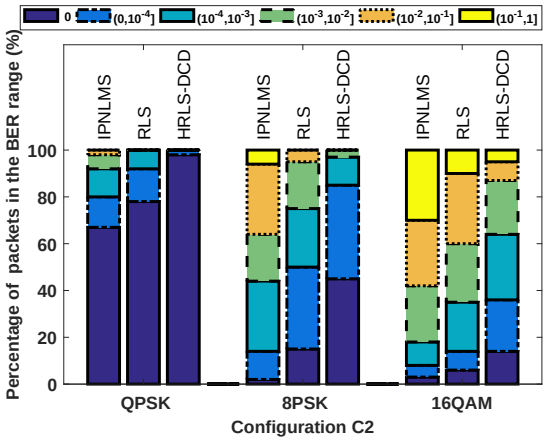

(b)

Fig. 6. Performance of the 2×4 MIMO system after 5 iterations for (a) configuration C1; (b) configuration C2.

iterations in terms of the percentages of packets with different BERs. In overall, all the three channel estimators with SD feedback can dramatically improve the performance of the turbo receiver, while a limited improvement is achieved by TEQs with channel estimators driven by the hard decision. The best performance is achieved by the TEQ with the SD-driven EW-HRLS-DCD based channel estimator; this is due to the reliable SD feedback and exploitation of sparsity of the UWA channel. The most of the performance gain is obtained after three iterations for all the receivers, and the improvement is negligible after the fifth iteration. For the IPNLMS-based TEQ after the fifth iteration, there are 27 data packets with zero BER out of the total 72 packets if the SD feedback is used, while there are only 9 zero-BER data packets for the hard decision feedback. For the RLS-based TEQ after the fifth iteration, there are 54 zero-BER data packets for the SD feedback, while there are 38 zero-BER data packets for the hard decision feedback. For the EW-HRLS-DCD-based TEQ after the fifth iteration, there are 61 zero-BER data packets for SD the feedback, and only 40 zero-BER data packets for the hard decision feedback. As opposed to the RLS- and EW-

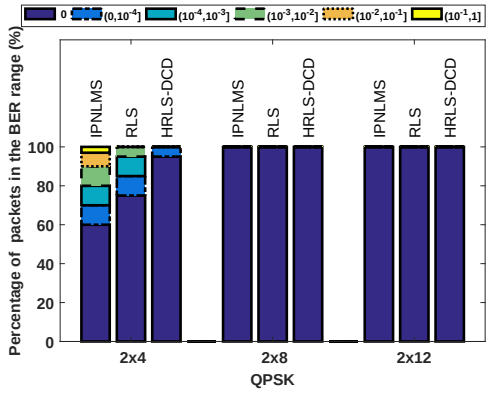

(a)

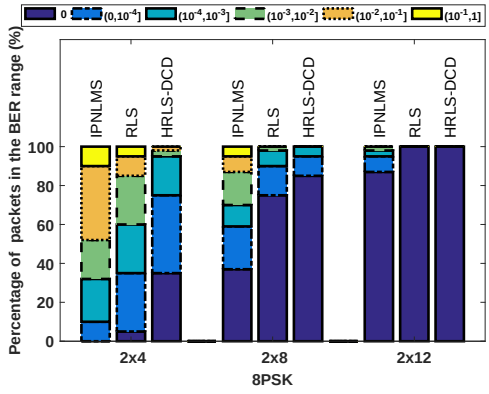

(b)

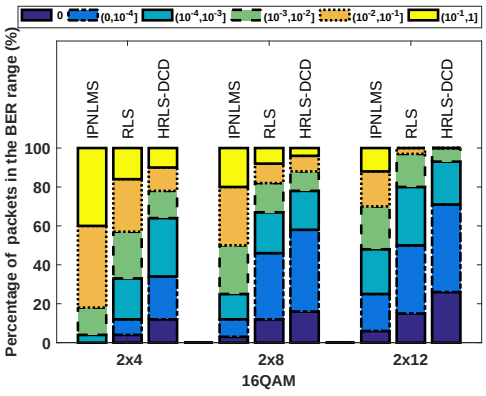

(c)

Fig. 9. Performance of the 2×4, 2×8 and 2×12 MIMO after 5 iterations with modulation: (a) QPSK, (b) 8PSK and (c) 16QAM.

HRLS-DCD-based channel estimators, no matter what kind of feedback is taken by the TEQ with the IPNLMS-based channel estimator, it always suffers from the convergence issue due to the short training sequence and fast time-varying UWA channel. However, the proposed EW-HRLS-DCD based channel estimator efficiently deals with this problem.

VII. Conclusion

In this paper, we have proposed and investigated a novel turbo equalizer for MIMO UWA systems with single-carrier

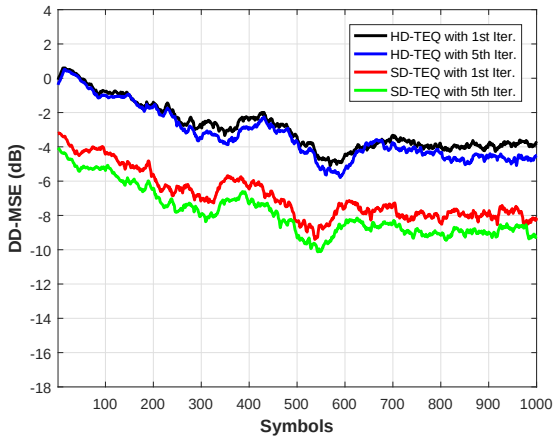

(a)

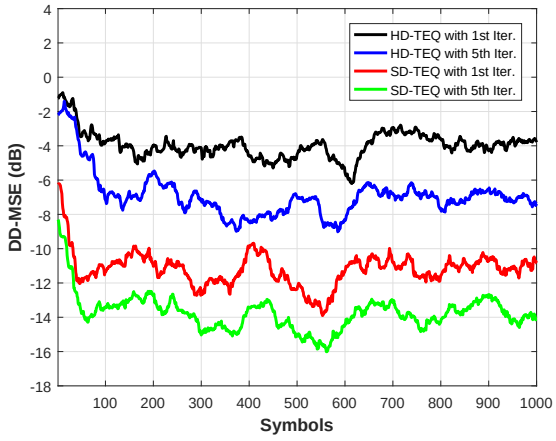

(b)

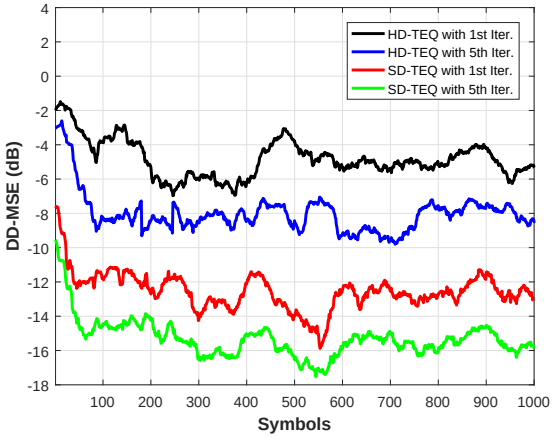

(c)

Fig. 10. DD-MSE of the equalizer output after first and fifth iteration. (a) IPNLMS, (b) RLS, (c) EW-HRLS-DCD.

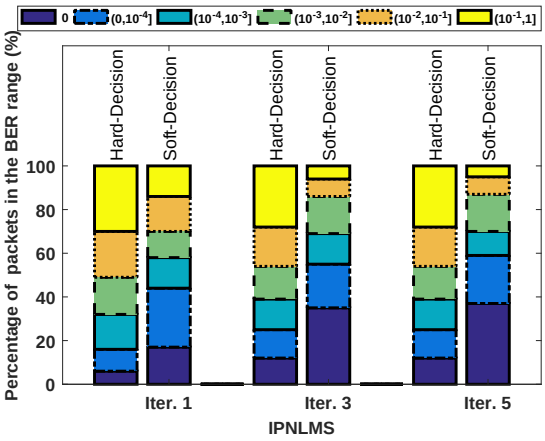

(a)

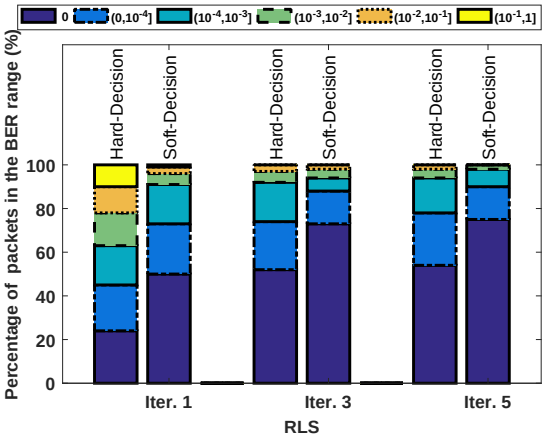

(b)

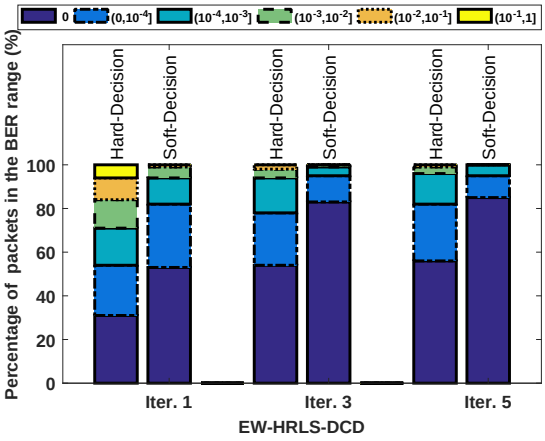

(c)

Fig. 11. Detection performance of the TEQs with the hard-decision and the *a posteriori* SD after first, third and fifth turbo iterations for the 2×8 MIMO setup: (a) IPNLMS, (b) RLS, (c) EW-HRLS-DCD.

modulation. A novel sparse adaptive filtering algorithm recently proposed for single input single output systems, and based on Homotopy iterations, DCD iterations, and reweighting, has been extended to efficiently estimate the fast time-varying sparse MIMO underwater acoustic channels. The reliable *a posteriori* soft decisions, instead of traditional *a priori* soft decisions or hard decisions, are feedback to the channel estimator and MMSE equalizer, leading to better accuracy of channel estimation and better performance of MMSE equalizer in

the proposed turbo MIMO equalizer. Through the experiment conducted in Songhua Lake in 2013, we have verified that the proposed turbo equalizer significantly outperforms the existing schemes based on the IPNLMS algorithm and conventional RLS algorithm with a lower complexity and better BER performance.

ACKNOWLEDGMENT

The work of Y. Zhang is supported by the National Natural Science Foundation of China (Grant No. 61471138, 50909029, and 61531012), China Scholarship Council Funding, Program of International S&T Cooperation (Grant No. 2013DFR20050), the Defense Industrial Technology Development Program (Grant No. B2420132004), the Acoustic Science and Technology Laboratory (2014). The work of Y. Zakharov is partly supported by the UK Engineering and Physical Sciences Research Council (EPSRC) through Grants EP/P017975/1 and EP/R003297/1.

REFERENCES

[1] M. Stojanovic, J. Catipovic, and J. Proakis, "Phase-coherent digital communications for underwater acoustic channels," *IEEE Journal of Oceanic Engineering*, vol. 19, no. 1, pp. 100-111, Jan. 1994.

[2] L. Freitag, M. Johnson and M. Stojanovic, "Efficient equalizer update algorithms for acoustic communication channels of varying complexity," *in OCEANS'97. MTS/IEEE Conference Proceedings*, Halifax, NS, Canada, vol. 1, pp. 580-585, Oct. 1997.

[3] C. Tsimenidis, O. Hinton, B. Sharif and A. Adams, "Spread-spectrum based adaptive array receiver algorithms for the shallow-water acoustic channel," *in Proc. IEEE Oceans'00 Conference*, Providence, RI, USA, vol. 2, pp. 1233-1237, Sept. 2000.

[4] J. Gomes and V. Barroso, "MIMO decision-feedback equalization with direct channel estimation," *in Proceedings of the 5th IEEE Workshop on Signal Processing Advances in Wireless Communications (SPAWC'04)*, Lisboa, Portugal, pp. 419-423, July 2004.

[5] H. C. Song, W. S. Hodgkiss, W. A. Kuperman, M. Stevenson, and T. Akal, "Improvement of time reversal communications using adaptive channel equalizers," *IEEE J. Oceanic Eng.*, vol. 31, no. 2, pp. 487-496, Apr. 2006.

[6] T. C. Yang, "A study of spatial processing gain in underwater acoustic communications," *IEEE J. Ocean. Eng.*, vol. 32, no. 3, pp. 689-709, Jul. 2007.

[7] K. Pelekanakis and M. Chitre, "Comparison of sparse adaptive filters for underwater acoustic channel equalization/estimation," *in Proc. IEEE Int. Conf. Commun. Syst. (ICCS)*, Singapore, Singapore, pp. 395C399, Nov. 2010.

[8] A. C. Singer, J. K. Nelson, and S. S. Kozat, "Signal processing for underwater acoustic communications," *IEEE Communications Magazine*, vol. 47, no. 1, pp. 90-96, 2009.

[9] J. Li and Y. V. Zakharov, "Multibranch Autocorrelation Method for Doppler Estimation in Underwater Acoustic Channels," *IEEE J. Ocean. Eng.*, vol. PP, no. 99, pp. 1-15, Nov. 2017.

[10] M. Stojanovic and J. Preisig, "Underwater acoustic communication channels: propagation models and statistical characterization," *IEEE Communications Magazine*, vol. 47, no. 1, pp. 84-89, January 2009.

[11] T. Arikan, T. Riedl, A. Singer and J. Younce, "Comparison of OFDM and single-carrier schemes for Doppler tolerant acoustic communications," *OCEANS 2015 - Genova*, Genoa, Italy, May 2015, pp. 1-7.

[12] B. Li, J. Huang, S. Zhou, K. Ball, M. Stojanovic, L. Freitag, and P. Willett, "MIMO-OFDM for High Rate Underwater Acoustic Communications," *IEEE Journal on Oceanic Engineering*, vol. 34, no. 4, pp. 634-644, Oct. 2009.

[13] M. Stojanovic, "Adaptive channel estimation for underwater acoustic MIMO OFDM systems," *in Proc. IEEE DSP/SPE Workshop 2009*, Marco Island, FL, Jan. 2009, pp. 132-137.

[14] Y. R. Zheng, J. Wu, and C. Xiao, "Turbo equalization for underwater acoustic communications," *IEEE Commun. Mag.*, vol. 53, no. 11, pp. 79-87, Nov. 2015.

[15] J. Li and Y. V. Zakharov, "Efficient Use of Space-Time Clustering for Underwater Acoustic Communications," *IEEE J. Ocean. Eng.*, vol. PP, no. 99, pp. 1-11, April 2017.

[16] J. Tao and Y. R. Zheng, "Turbo detection for MIMO-OFDM underwater acoustic communications," *Int. J. Wireless Inf. Netw.*, vol. 20, no. 1, pp. 27-38, Mar. 2013.

[17] K. Tu, D. Fertonani, T. M. Duman, M. Stojanovic, J. G. Proakis, and P. Hursky, "Mitigation of intercarrier interference for OFDM over time-varying underwater acoustic channels," *IEEE J. Ocean. Eng.*, vol. 36, no. 2, pp. 156-171, Apr. 2011.

[18] Y. V. Zakharov and A. K. Morozov, "OFDM transmission without guard interval in fast-varying underwater acoustic channels," *IEEE J. Ocean. Eng.*, vol. 40, no. 1, pp. 144-158, Jan. 2015.

[19] L. Cannelli, G. Leus, H. Dol, and P. van Walree, "Adaptive turbo equalization for underwater acoustic communication," *in Proc. MTS/IEEE OCEANS Conf.*, Bergen, Norway, pp. 1-9, Jun. 2013.

[20] J. W. Choi, T. J. Riedl, K. Kim, A. C. Singer, and J. C. Preisig, "Adaptive linear turbo equalization over doubly selective channels," *IEEE J. Ocean. Eng.*, vol. 36, no. 4, pp. 473-489, Oct. 2011.

[21] C. Laot, N. Beuzeulin, and A. Bourre, "Experimental results on MMSE turbo equalization in underwater acoustic communication using high order modulation," *in Proc. MTS/IEEE OCEANS Conf.*, Seattle, WA, USA, Sep. 2010, pp. 1-6.

[22] C. Laot and R. L. Bidan, "Adaptive MMSE turbo equalization with high order modulations and spatial diversity applied to underwater acoustic communications," *in Proc. 11th Eur. Wireless Conf. Sustain. Wireless Technol.*, Vienna, Austria, Apr. 2011, pp. 1-6.

[23] M. Qingwei, H. Jianguo, H. Jing, H. Chengbing, and M. Chuang, "An improved direct adaptive multichannel turbo equalization scheme for underwater communications," *in Proc. MTS/IEEE OCEANS Conf.*, Yeosu, South Korea, May 2012, pp. 1-5.

[24] J. Benesty and S. L. Gay, "An improved PNLMS algorithm," *IEEE ICASSP-02*, Orlando, FL, USA, May 2002, vol. 2, pp. 1881-1884.

[25] A. Yellepeddi and J. C. Preisig, "Adaptive equalization in a turbo loop," *IEEE Trans. Wireless Commun.*, vol. 14, no. 9, pp. 5111-5122, Sep. 2015.

[26] M. Tüchler and J. Hagenauer, "Linear time and frequency domain turbo equalization," *Proc. IEEE Veh. Technol. Conf.*, vol. 2, pp. 1449-1453, May 2001.

[27] J. Tao, J. Wu, Y. R. Zheng and C. Xiao, "Enhanced MIMO LMMSE turbo equalization: Algorithm simulations and undersea experimental results," *IEEE Trans. Signal Process.*, vol. 59, no. 8, pp. 3813-3823, 2011.

[28] Y. V. Zakharov and V. H. Nascimento, "Homotopy RLS-DCD adaptive filter," *In Proceedings of the Tenth International Symposium on Wireless Communication Systems (ISWCS)*, Ilmenau, Germany, pp. 1-5, Aug. 2013.

[29] J. Li and Y. V. Zakharov, "Sliding-window homotopy adaptive filter for estimation of sparse UWA channels," *in 2016 IEEE Sensor Array and Multichannel Signal Processing Workshop (SAM)*, Rio de Janerio, Brazil, pp. 1-4, 10-13 July 2016.

[30] J. Li and Y. V. Zakharov, "Sliding window adaptive filter with diagonal loading for estimation of sparse UWA channels," *in OCEANS 2016 - Shanghai*, Shanghai, China, pp. 1-5, 10-13 April 2016.

[31] Z. Chen, Y. R. Zheng, J. Wang and J. Song, "Frequency domain turbo equalization with iterative channel estimation for single carrier MIMO underwater acoustic communications," *Proc. IEEE Veh. Technol. Conf.*, Boston, MA, USA, Sep. 2015, pp. 1-5.

[32] J. Zhang and Y. R. Zheng, "Bandwidth-efficient frequency-domain equalization for single carrier multiple-input multiple-output underwater acoustic communications," *J. Acoust. Soc. Amer.*, vol. 128, no. 5, pp. 2910-2919, 2010.

[33] Z.-H. Wang, J. Huang, S. Zhou, and Z. Wang, "Iterative Receiver Processing for OFDM Modulated Physical-Layer Network Coding in Underwater Acoustic Channels," *IEEE Transactions on Comm.*, vol. 61, no. 2, pp. 541-553, Feb. 2013.

[34] J. Tao, "Single-carrier frequency-domain turbo equalization with various soft interference cancellation schemes for MIMO systems," *IEEE Trans. Commun.*, vol. 63, no. 9, pp. 3206-3217, 2015.

[35] W. Duan and Y. R. Zheng, "Bidirectional Soft-Decision Feedback Equalization for Robust MIMO Underwater Acoustic Communications," *MTS/IEEE OCEANS*, St. Johns, NL, Canada, Sep. 14-18, 2014, pp. 1-6.

[36] W. Duan and Y. R. Zheng, "Bidirectional Soft Decision Feedback Turbo Equalization for MIMO Systems," *IEEE Trans. Veh. Techno.*, vol. 65, no. 7, pp. 4925-4936, July 2016.

[37] W. Duan, J. Tao and Y. R. Zheng, "Efficient Adaptive Turbo Equalization for Multiple-Input-Multiple-Output Underwater Acoustic Communications," *IEEE J. Ocean. Eng.*, vol. PP, no. 99, pp. 1-13, July 2017.

[38] Z. Yang and Y. R. Zheng, "Iterative channel estimation and turbo equalization for multiple-input multiple-output underwater acoustic communications," *IEEE J. Ocean. Eng.* vol. 41, no. 1, pp. 232-242, 2016.

[39] S. Haykin, *Adaptive Filter Theory*, 4th Edition, Prentice Hall Inc., 2002.

[40] J. G. Proakis, *Digital Communications*, 4th ed. New York, NY, USA: McGraw Hill, 2000.
[41] T. K. Akino, "Optimum-weighted RLS channel estimation for rapid fading MIMO channels," *IEEE Trans. Wireless Commun.*, vol. 7, no. 11, pp. 4248-4260, Nov. 2008.
[42] T. K. Akino, A. F. Molisch, R. Annavajjala, P. Orlik, M. O. Pun, "Order-Extended Sparse RLS Algorithm for Doubly-Selective MIMO Channel Estimation," *IEEE International Conference on Communications (ICC)*, Kyoto, Japan, Jun. 2011, pp. 1-6.
[43] J. Tao, Y. R. Zheng, C. Xiao, and T. Yang, "Robust MIMO underwater acoustic communications using turbo block decision-feedback equalization," *IEEE J. Ocean. Eng.*, vol. 35, no. 4, pp. 948-960, Oct. 2010.
[44] Y. V. Zakharov, G. White, and J. Liu, "Low complexity RLS algorithms using dichotomous coordinate descent iterations," *IEEE Transactions on Signal Processing*, vol. 56, no. 7, pp. 3150-3161, July 2008.
[45] M. Kocic, D. Brady, and M. Stojanovic, "Sparse equalization for real-time digital underwater acoustic communications," *in Proc. 1995 MTS/IEEE OCEANS*, San Diego, California, USA, Oct. 1995, vol. 3, pp. 1417-1422.
[46] Y. V. Zakharov and A. K. Morozov, "Adaptive sparse channel estimation for guard-free OFDM transmission in underwater acoustic channels," *in Proc. 12th Eur. Conf. Underwater Acoust.*, Corfu, Greece, Jun. 2013, pp. 1347-1354.
[47] D. Donoho, "Compressed sensing," *IEEE Trans. Inf. Theory*, vol. 52, no. 4, pp. 1289-1306, Apr. 2006.
[48] C. R. Berger, Z.-H. Wang, J.-Z. Huang, and S. Zhou, "Application of Compressive Sensing to Sparse Channel Estimation," *IEEE Communications Magazine*, vol. 48, no. 11, pp. 164-174, Nov. 2010.
[49] J. Huang, J.-Z. Huang, C. R. Berger, S. Zhou, and P. Willett, "Iterative sparse channel estimation and decoding for underwater MIMO-OFDM," *EURASIP Journal on Advances in Signal Processing*, vol. 2010, Article ID 460379, 11 pages, 2010.
[50] B. Babadi, N. Kalouptsidis, and V. Tarokh, "SPARLS: The sparse RLS algorithm," *IEEE Trans. Signal Process.*, vol. 58, no. 8, pp. 4013-4025, Aug. 2010.
[51] E. M. Eksioglu and A. K. Tanc, "RLS algorithm with convex regularization," *IEEE Signal Process. Let.*, vol. 18, no. 8, pp. 470-473, Aug. 2011.
[52] Y. V. Zakharov and V. H. Nascimento, "DCD-RLS adaptive filters with penalties for sparse identification," *IEEE Trans. Signal Process.*, vol. 61, no. 12, pp. 3198-3213, Jun. 2013.
[53] Y. V. Zakharov and V. Nascimento, "Sparse RLS adaptive filter with diagonal loading," *in 46th Asilomar Conference on Signals, Systems and Computers*, Pacific Grove, CA, USA, Nov. 2012, pp. 806-810.
[54] Y. V. Zakharov and T. C. Tozer, "Multiplication-free iterative algorithm for LS problem," *Electron. Lett.*, vol. 40, no. 9, pp. 567-569, Apr. 2004.
[55] M. Tüchler, R. Koetter and A. C. Singer, "Turbo equalization: principles and new results," *IEEE Trans. Commun.*, vol. 50, no. 5, pp. 754-767, May 2002.
[56] M. Tüchler, A. C. Singer and R. Koetter, "Minimum mean square error equalization using a priori information," *IEEE Trans. Signal Process.*, vol. 50, no. 3, pp. 673-683, 2002.
[57] R. Otnes and M. Tüchler, "Soft iterative channel estimation for turbo equalization: comparison of channel estimation algorithms," *in The 8th International Conference on Communication Systems (ICCS 2002)*, Singapore, Singapore, vol. 1, pp. 72-76, Nov. 2002.
[58] R. Otnes and M. Tüchler, "Iterative channel estimation for turbo equalization of time-varying frequency selective channels," *IEEE Trans. Wireless Commun.*, vol. 3, no. 6, pp. 1918-1923, Nov. 2004.